We thank the reviewers for their suggestions, which certainly helped us improving the manuscript. We tried to account for many of the points which are listed below in the text. In the following the reviewer's comments are presented in italics, the author answer with normal letters in blue and the modifications on the manuscript with bold blue letters.

Anonymous Referee #1

General points

In Section 2 the authors report about trace gas measurements and show a global distribution in Figure 1. These measurements and Figure do not have an impact on the further analysis and inversion of the lidar data and should be omitted to make space for some other analysis which are missing in this paper, for example a case study of urban/industrial aerosols and more information about the mixed biomass burning layers.

In section 2.4, paragraph 4, we report on trace gas measurements. These measurements were actually used to classify the origin of the aerosols in each of our case study of table 1. The trace gas measurements are part of our analysis on the categorization of urban/industrial aerosol type. In particular, as clearly mentioned in the manuscript '15 min data were averaged for the extent of measurement time for each of the measurements periods (Table 1). For instances where the combined use of trajectory analysis and fire hotspots did not indicate the presence of biomass burning aerosols we checked whether the measured NOx, SO2 or H2S concentrations were higher than the seasonal mean values of that measured for the entire period of the EUCAARI campaign. These seasonal mean values are presented in Laakso et al. (2012). In addition, when the trace gases concentrations were lower than the mean seasonal values measured during the EUCAARI campaign and biomass-burning activity or desert dust advection were absent, we checked if the daily concentration of the trace gases exceeded the mean critical values.'

Figure 1 show the global map of long-term average tropospheric NO_2 column derived from SCIAMACHY data from August 2002 to March 2012. We agree with the reviewer that this figure do not have an impact on further data analysis but this figure is used to demonstrate the distribution and intensity of urban / industrial aerosols in the region. It is used in the section 2.1 which is the description of measurement site and we believe that helps (together with Figure 2) the reader to understand the existence of the 2 dominant aerosol sources. For this reason we prefer to keep Figure 1.

The authors state that the uncertainties of the extinction coefficient are in the order of 10-30%. Later they make assumptions of differences in the size of the particles mainly indicated by differences of the Angstroem exponent. How are these assumptions and the Angstroem exponents affected by the general uncertainties of the extinction coefficient?

We thank the reviewer#1 for the comment. In section 2,2 we briefly state the errors in backscatter, extinction, depolarization and lidar ratio, but we missed to state the error in the Ångström exponent. We now clearly state the error also in the Ångström exponent. '**The overall relative errors of the lidar-derived aerosol properties range between 5%-15% for the backscatter coefficients, 10%-30% for the extinction coefficients, 20%-40% for the Ångström exponents, 15%-40% for the lidar ratios and approximately 5%-10% for the linear particle depolarization ratio (Hänel et al., 2012)**.' Also a reference ('Wagner et al., 2008') is cited in the revised manuscript where the error in Ångström exponents and how these errors are influenced by errors in aerosol optical depths, is discussed in detail.

The authors should report more about their uncertainties; what do they consider for their analysis of the uncertainties. Which parameters are not considered? If possible they should do an error analysis for all reported and considered measurement cases.

A detailed error analysis for FMI-Polly^{XT} systems has not been done, and it would take up an entire new publication including the error propagation formalisms, the separation of statistical and systematic errors, Monte-Carlo approach and known uncertainties for all of the channels. However some discussion on the error

analysis are already made on *Baars et al. 2016* and on *Engelmann et al., 2016* and these two publications are cited in the revised manuscript.

Baars, H., Kanitz, T., Engelmann, R., Althausen, D., Heese, B., Komppula, M., Preißler, J., Tesche, M., Ansmann, A., Wandinger, U., Lim, J.-H., Ahn, J. Y., Stachlewska, I. S., Amiridis, V., Marinou, E., Seifert, P., Hofer, J., Skupin, A., Schneider, F., Bohlmann, S., Foth, A., Bley, S., Pfüller, A., Giannakaki, E., Lihavainen, H., Viisanen, Y., Hooda, R. K., Pereira, S. N., Bortoli, D., Wagner, F., Mattis, I., Janicka, L., Markowicz, K. M., Achtert, P., Artaxo, P., Pauliquevis, T., Souza, R. A. F., Sharma, V. P., van Zyl, P. G., Beukes, J. P., Sun, J., Rohwer, E. G., Deng, R., Mamouri, R.-E., and Zamorano, F.: An overview of the first decade of PollyNET: an emerging network of automated Raman-polarization lidars for continuous aerosol profiling, Atmos. Chem. Phys., 16, 5111-5137, doi:10.5194/acp-16-5111-2016, 2016.

Engelmann, R., Kanitz, T., Baars, H., Heese, B., Althausen, D., Skupin, A., Wandinger, U., Komppula, M., Stachlewska, I. S., Amiridis, V., Marinou, E., Mattis, I., Linné, H., and Ansmann, A.: The automated multiwavelength Raman polarization and water-vapor lidar PollyXT: the neXT generation, Atmos. Meas. Tech., 9, 1767–1784, doi:10.5194/amt-9-1767-2016, 2016.

In this study we limited ourselves to the general description of the error sources of FMI-Polly^{XT} and to those we can actually specify. Thus we include a small paragraph in the revised manuscript:

The uncertainties affecting the retrieval of extinction and backscatter coefficients, and thus the calculation of lidar ratio and Ångström exponents are mainly due: to the statistical error due to signal detection,the systematic error associated with the estimation of the atmospheric moleculat number density from the pressurte and temperature profiles, the systematic error associated with the evaluation of the aerosol scattering wavelength dependence, the systematic error for overlap function, the errors introduced by operation procedure such as signal binning (smoothing) and averaging accumulating lidar returns.

The authors classify there aerosol types mainly based on trajectory analysis. How these classifications are connected with lidar based classification schemes (Burton et al., 2012, Gross et al., 2013, or at 355 nm: Gross et al., 2015, Illingworth et al., 2015)? Please add this in your publication.

The aerosol type identification as described in section 2.4 (Aerosol classification) is based on three tools.

1. Backward trajectories (paragraph 2 of section 2.4)
2. Modis fire hot spots (paragraph 3 of section 2.4)
3. Trace gas measurements criteria (paragraph 4 of section 2.4)

We would like to make clear at this point that the purpose of this study is not to classify our measurements based on the post-processing of lidar data products but to pre classify our layers and then calculate and present our averaged intensive properties of the different types of aerosol layers in the region of South Africa. Also, at the last part of our study we compare our results with other studies (also those proposed by the reviewer#1).

How is the assumption of less absorption for biomass burning conform with the lidar ratio of 52 sr compared to 92 sr for industrial/urban aerosols?

In section 3 a case study of biomass burning aerosols is presented and discussed. In the layer between 1090m and 1900m, high values of the lidar ratio of 96 ± 5 sr at 355 nm and 89 ± 5 sr at 532 nm are calculated which indicate that the smoke particles inside this layer were most likely highly light-absorbing . The single scattering albedo for this particular layer was 0.86 at 532 nm which is also indicates relatively strong-absorbing aerosols.

In Table 2 and 3 we also present the mean aerosol properties for the three aerosol types. The biomass burning particles were found to be larger and slightly less absorbing compared to urban/industrial aerosols. Our results for lidar ratios and single scattering albedo in general were within the same range of previously reported values. The slightly higher values of single scattering albedo for biomass burning aerosols (0.90 ± 0.06) compared with the single scattering albedo of urban/industrial aerosols (0.87 ± 0.06) is caused by the lower imaginary part of the retrieved complex refractive index of biomass burning aerosols (0.016 (± 0.011)i) compared with that of

urban/industrial aerosols (0.021 (± 0.010)i). The values are presented in Table 3. Here the retrieved single scattering albedo is used as a metric of the absorption of the aerosols (and is not an assumption as the reviewer suggested). The lidar ratio is a parameter that is affected by the absorption, but it is also depending on the size of the particles. Smoke particles were found larger (effective radius 0.17 ± 0.04) than urban/industrial aerosols (effective radius 0.10 ± 0.03) which have an impact on backscatter efficiency and thus on lidar ratio values. Taking these into account, together with the standard deviation of the single scattering albedo (± 0.06) we think that our results are reasonable.

How do you calibrate your depolarization measurements? How does this calibration method affect your results? Please report in you publication.

Depolarization measurements at 355 nm are perfomed. The Rayleigh calibration method was applied within the data analysis under the assumption of pure Rayleigh depolarization in an aerosol-free height range (Behrendt and Nakamura, 2002). However, we should note here that the FMI Polly^{XT}system has been upgraded and we now perform measurements at 532 nm with the Δ90◦ -calibration (formerly known as ±45◦ -calibration method (Freudenthaler et al., 2009).

How do the uncertainties in the single measurement parameters affect the result of the inversion algorithm?

The effect of the uncertainties of the single measurement parameters to the results of the inversion algorithim is discussed in detail in Müller et al., 2001 and is briefly reported in section 2.3: '**A minimum of three backscatter coefficients (355, 532, and 1064 nm) and two extinction coefficients (355 and 532 nm), with measurement errors less than 30%, are required as input in order to obtain microphysical results that have reasonably low uncertainties (Müller et al., 2001). The selection of the individual inversion solutions is based on the concept that the back-calculated optical data should agree with the original data within the limits of the measurement errors, and that a pre-selected discrepancy level, which is an output parameter of the inversion algorithm (Müller et al., 1999a), is not exceeded.**'

Are the +/- values the mean uncertainties or the standard deviation? Please add this information in your publication.

The +/- values are the standard deviation. The information is already provided in the text and the captions of the Tables 2 and 3 as well as in the Figure 7 (previously Figure 8).

Instead of showing the trace gas measurements the authors should show a figure with AOD, extinction coefficient or backscatter coefficient for one day prior to one day after their biomass burning case study as that seems to be an important point and mentioned in the text.

We would like to keep Figure 1 because we think that helps the reader to understand the dominant aerosol sources in the region. In Figure 4 (previously Figure 5) we now include the mean backscatter coefficient at 532 nm for one day prior and one day after the biomass burning case study as suggested by the reviewer. We do not include all three wavelengths to keep the figure as clear as possible.

A case study showing a urban/industrial aerosol case and a mixed biomass burning case is missing. Especial important would be to see the differences in transport way, extinction coefficient or AOD, and layering for the different cases.

We thank the reviewer for the comment. In this study we present our results on 38 aerosol layers, from which 17 are referring to urban/industrial, 14 to biomass burning and 7 to mixed of biomass burning with desert dust aerosols. We think that the measurement example is a good and common way to show the typical products of our system and to demonstrate the methodology used to derive the optical aerosol properties. Differences in transport way, extinction and backscatter coefficients as well as layering structures are observed at all cases, also within one cluster of aerosol types. Some information on the aerosol structure for each of the layer analyzed is already given in the Table 1 (bottom and top of each layer observed). Mean extinction coefficient at 355 nm and 532 nm for each of the layer observed are now add in the Table 1 of the revised manuscript as

suggested by the reviewer#1. The respective aerosol optical depths at 355 nm and 532 nm can now be easily retrieved from the mean extinctions coefficients and geometrical information provided in the Table 1.

The authors should give more evidence that the mixed biomass burning cases are not miss-classified. The measurements presented (e.g. in Figure 5) show almost the same values as what is classified as aged biomass burning aerosols in Illingworth et al., 2015. Furthermore Amiridis et al., 2009 reported that the optical properties of biomass burning aerosols alter during aging.
It is also not clear to me what really should happen with the dust particles. How would this affect their shape and optical properties? The authors should give more references and evidence for their assumption.
Thank you the reviewer for the comment. Illingworth et al., 2015 among other types, studied the intensive properties of aged boreal biomass burning aerosols and found depolarization values at 355 nm between 10 – 11 %. This range value is indeed very similar with our values for mixed biomass burning / desert dust particles. However, the lidar ratio values given by illingworth et al., 2015 for aged boreal biomass burning (35 – 50 sr) is much smaller than the values reported in this study (59 – 90 sr).
Amiridis et al., 2009 reported a wide range of lidar ratio values at 355 nm for biomass burning aerosols and our values are within this range. They also studied the relation between backscatter related Ångström exponent and the age of carbon monoxide from the emissions. Our results on the intensive parameters (both for biomass burning and mixed aerosols) are in agreement with those reported by Amiridis et al., 2009. Although we should note that we report Ångström exponent related to extinction and not related to backscatter. The main difference between the biomass burning and biomass burning missed with desert dust is the depolarization ratio values and this is a parameter that is not reported in Amiridis et al. 2009.
According to our trajectory analysis there is certainly evidence of the transport of biomass burning aerosols in the measurement site. The smoke is relatively fresh (less than 3-day-old smoke plume). A relation between travel time and Ångström exponent was not found in our dataset, and we believe that the travel time is relatively short and thus don't make possible to see large differences in the intensive properties. The transport paths are different even in one cluster of aerosol types and thus we do not provide such a Figure.
We agree with the reviewer that the evidence of desert dust transport in our study is not so clear and thus we changed the name of this aerosol type to mixed aerosols. The mixing state of the aerosols is possible from desert dust but also industrial aerosols can not be excluded, especially in this region.

Is the assumption of mixture of dust and biomass burning also conforming in the lidar ratio? The authors report quite low lidar ratios compared to the referenced studies which they use as hint for their assumption. How these assumptions do are supported by results of optical modelling (e.g. Gasteiger et al., 2011 for the referenced measurements)?
Considering the last points a detailed case study should be added. This case study should also include information (satellite / reports) of dust activation and a connection to trajectory analysis including the mixing layer height and trajectory height.
A new publication including the mixing of desert dust, urban aerosols and biomass burning aerosols during biomass burning period will follow in the near future. The contribution of each of these aerosol types will be quantified using the information of particle depolarization ratio. In the present study we have changed the mixtrure of dust and biomass burning to a mixed state of aerosols, since there is not yet enough proof of dust activation. However, the larger depolarization values found for this mixture type cannot be explained by the age of the smoke plume as explained in the previous answer.
The lidar ratio values is very well compared with the mixture type as shown in Figure 7. The lower depolarization values and larger Ångström exponent values compared to the literature values can be explained both from the different kind of dust and smoke as well as from the different (less) contribution of the dust to the mixing state of aerosols.

Specific comments:

Abstract:

Change 'proper ties' to 'properties'.

done

Change 'single scattering, albedo' to 'single scattering albedo'.

done

Why not give also the lidar ratio at 532 nm?

done

AE for biomass burning is not consistent with Table 2.

Thank you the reviewer for the comment. The reviewer is right. In the new manuscript the AE for biomass burning is consistent with Table 2

Section 2:

Which is the range of full overlap?

Usually the overlap function is equal to 0.7 at heights between 300-500 m. In this study, we only report aerosol layers in the range of full overlap.

Section 3:

Please constrain your assumption of 'fresh smoke'; give references.

The travel time of air masses studied here is less than 3-day-old

Section 4:

Do you really mean anthropogenic here? Give references for this assumption.

Thank you for the reviewer's comment. It was not cleared in the manuscript that we were referring to our results and not to the literature. In the revised manuscript we have replaced the sentence 'Anthropogenic aerosol layers are characterized by lower lidar ratios in the range between 41 and 59 sr' with 'Urban / Industrial aerosol layers were found to have lower lidar ratio values in the range between 41 and 59 sr at 355 nm'.

Figure 2:

Add 'of fire' to indicate which hot spots you mean.

done

Figure 3:

How does a quicklook with 15 km height resolution go conform with a reported vertical resolution of 30 km?

Thank you for the reviewer's comment. The vertical resolution is 30 m and not 15 m. In the revised manuscript the correct height resolution is reported in section 2.2. Figure 3 is deleted in the revised version as reviewer #3 has proposed.

Figure 4 / Section 3:

I cannot see that airmasses are coming either from northeasterly or northwesterly direction. A more detailed trajectory analysis including also the mixing layer height and trajectory height along the way would give more evidence at which part of the transport aerosol uptake took place.

Thank you the reviewer for the comment. In the new manuscript we have change Figure 4. In Figure 3a (previously Figure 4) we present the fire hot spots, and in Figure 4b we present the four day back-trajectories along with the trajectory height and mixing layer height as suggested by the reviewer. The discussion of the trajectory has also changed in the revised paper: 'MODIS fire hotspots product reveal that several fires were active during the period 28th of September 2010 – 1st of October 2010 as shown in Figure 3 (a). In Figure 3 (b), four-day backward trajectories arriving at Elandsfontein on 1st of October 2010 at 00:00 are presented. The trajectories are computed for arrival heights of the bottom, center and top of the observed layer. The trajectory

analysis along with MODIS fire hotspots reveals that the air masses are highly possible to carry smoke particles at Elandsfontein on the day of the measurement. '

Figure 5:
How do you explain the increase of the backscatter ratio at 355 nm with height?
Thank you the reviewer for the comment. There is indeed an increase of backscatter coefficient at 355 nm. This is partially caused by the vertically smoothing applied in our analysis. This increase is small and inside the order of the error bars. In our analysis we don't take into account the lower part of the profile. Only the mean values of optical properties of the aerosol layer (grey region) were used and looking also the vertical distribution of lidar ratio and Ångström exponent there is only a small effect in the averaged values of the layer taken into account.

What is the vertical resolution of this data?
The vertical resolution of the data is 30 m as reported in section 2.2. We have applied a smoothing of 9 points (270 m) in the specific case study.

Figure 7:
Change your labeling from 'Depolarazation' to 'Depolarization'.
Thank you the reviewer for the comment. Done

Figure 8:
The labeling is not readable. Please change.
Thank you the reviewer for the comment. Done

Anonymous Referee #2

Main comment The manuscript presents an interesting study of the atmospheric aerosol features in South Africa. The study area deserves some attention due to the variety of aerosols that affect the region. The approach used implies the processing of backscattering and absorption coefficients derived from Raman lidar processing. The presentation of the study is appropriate; the description of the analyses includes the estimation of uncertainties. The discussion of the results has been done with a good review of previous works in the field. The manuscript is suitable for publication after minor revisions.

Particular comments.
The study includes the statistical analyses in order to characterize the properties associated to different aerosol types. A study case if selected to illustrate one of the categories of aerosols considered in the classification. In this sense, I would ask the authors why they did not include study cases illustrating the two other categories?
In this study we present our results on 38 aerosol layers, from which 17 are referring to urban/industrial, 14 to biomass burning and 7 to mixed of biomass burning with desert dust aerosols. We think that the measurement example is a good and common way to show the typical products of our system and only used to demonstrate the methodology followed to derive the optical aerosol properties. Some information on the aerosol structure for each of the layer analyzed is already given in the Table 1 (bottom and top of each layer observed). Mean extinction coefficient at 355 nm and 532 nm for each of the layer observed are also added in the Table 1 of the revised manuscript as suggested by the reviewer#1. The intensive aerosol optical properties and some microphysical properties are also shown in Figures 5, 6 and 7 for each of the cases analyzed. The air mass transport paths are different also within one cluster of aerosol types, and thus we believe that the presentation of two additional case studies will not improve our publication.

Among the variables used for the characterization of the aerosol types it is include the linear particle depolarization ratio. The authors quote the uncertainty of this uncertainty in a relatively small value. I guess would be this quotation just in case the considered the papers would be used for the quotation of the linear particle depolarization ratio?

We are not sure that we have understood the reviewer's comment.

A final point is concerned with the size of some figures that are really small and difficult to interpret due to the size of the letter. This is the case for´figure 5 but specially for figure 8.

In the revised manuscript we enlarge the axis titles and numbers of Figure 5 and Figure 8

Another issue, related to Figure 8, is that in their use in the discussion of results the authors did not include any particular comments on some of the cases displayed.

There are many statistics of intensive aerosol properties for different aerosol types in the world available for comparison and discussion. We believe that Figure 7 (previously Figure 8) provides some of the basic literature values, and we discuss most of the references included in Figure 7. We use the literature values in general to compare them with our results. For example we believe it is enough to report that the lidar ratio at 355 nm shows similar values for urban / industrial aerosols in various regions of the world (as shown in Figure 7, left corner), while for biomass burning aerosol where the range of the reported literature values for the lidar ratio at 355 nm are wider, we explicitly compare our results with individual studies.

Anonymous Referee #3

I think the paper can be publishes after minor revisions.

Comments: Not sure that this fig.2 is really necessary. The plots are too small to see details and information from this figure is not used for analysis.

Figure 2 is being discussed in section 2.1 where the measurement site is described. We would like to keep the figure because we believe that in this way the dominant source of biomass burning is presented in a better way. However, we agree with the reviewer that the plot is small to see details and for that reason we change the structure of the Figure in the revised manuscript.

Fig.3 doesn't present much information. May be it is better just to show vertical profile of backscattering instead?

Thank you the reviewer for the comment. The plot indeed doesn't give much information. Figure 3 has been deleted from the revised manuscript. The basic information of the figure is given in the text and we also provide the link where the temporal development of the range corrected signals of all channels could be found. The vertical profile of backscatter is given in Figure 4 (previously number Figure 5)

For backscattering calculation at 1064 Klett method was used. The lidar ratios in thiswork present strong variation, so the used values of lidar ratio at 1064 should be discussed.

Thank you for the reviewer's comment. We have add a paragraph to discuss how the backscatter at 1064 nm is retrieved. To vertically retrieve the backscatter coefficient at 1064 nm we use Fernald-Klett method (Fernald, 1984; Klett, 1981). With this method the particle backscatter coefficient is derived applying a backward iteration starting at a chosen reference height. The method requires independent information on the lidar ratio and on the reference value of the particle backscatter coefficient. The cases analyzed here are night-time measurements and the retrieved backscatter at 1064 nm was also evaluated by the Raman method (Ansmann et al. , 1992) using also the signal from the Nitrogen Raman channel at the 607 nm.

p. 35248. Ln.17. "Model calculations show that a deviation from the spherical shape can efficiently increase particle backscattering: : :" I think this statement is wrong. Nonspherical particles have no peaking in backward direction so backscattering is lower.

Thank you the reviewer for the comment. The statement is deleted in the revised manuscript

Fig.8. Text is very small, difficult to read.

The Text in Figure 7 (previously Figure 8) is enlarged in the revised manuscript.

Table 2. Angstrom exponent for biomass burning is 1.7, while for the mixture of biomass burning and desert dust is 2.0. It is strange, because big dust particles should decrease EAE.

Thank you the reviewer for the comment. The Ångström exponent for biomass burning is 1.7, while for the mixture of biomass burning and desert dust is 2.0. This lead to effective radius of 0.17 ± 0.04 μm and 0.13 ± 0.03 μm respectively. We should firstly note that in the revised manuscript the third aerosol type is referred to mixture state of aerosols in general and not to mixing of desert dust and biomass burning aerosols. According to trajectory analysis desert dust particles could have been transported on the measurement site but there is not enough proof of dust activation. Also, the influence of the industrial aerosols cannot be excluded. The effect of a continuous influence of industrial properties in our measurements and results could change the size (Ångström exponent) and shape(depolarization ratio) of our mixture aerosols. A new publication including the mixing of desert dust, urban aerosols and biomass burning aerosols during biomass burning period will follow in the near future. The contribution of each of these aerosol types will be quantified using the information of particle depolarization ratio and a detail analysis on the size distribution and Ångström exponent will be discussed.

Lidar ratios for mixture of biomass burning and desert dust at 355 and 532 nm differ more than twice. It should be discussed.

Thank you for the reviewer last comment! The value of median lidar ratio at 355 nm is wrong. The mistake was done by copying the maximum value (90 sr, see also Figure 5 (previously Figure 6)) of lidar ratio at 355 nm instead of copying the median value (73 sr). The mistake is corrected in the Table 2 of the revised manuscript and the other numbers of the Table 2 were also checked.

Optical and microphysical characterization of aerosol layers over South Africa by means of multi-wavelength depolarization and Raman lidar measurements

E. Giannakaki[1,~~2~~a], P.G. van ~~Zyl~~[3]Zyl[2], D. ~~Müller~~[4]Müller[3], D. ~~Balis~~[5]Balis[4] and M. Komppula[1]

(1){Finnish Meteorological Institute, P.O.Box 1627, FI-70211, Kuopio, Finland}

~~(2){Department of Environmental Physics and Meteorology, Faculty of Physics, University of Athens, Athens, Greece}*~~

(~~3~~2){Unit for Environmental Sciences and Management, North-West University, Potchefstroom, South Africa}

(43){School of Physics, Astronomy and Mathematics, University of Hertfordshire, Hatfield, United Kingdom}

(~~5~~4){Laboratory of Atmospheric Physics, Thessaloniki, Greece}

~~* in leave of absence~~

[a] on leave from {Department of Environmental Physics and Meteorology, Faculty of Physics, University of Athens, Athens, Greece}

Correspondence to: Elina Giannakaki (eleni.giannakaki@fmi.fi)

Abstract

Optical and microphysical properties of different aerosol types over South Africa measured with a multi-wavelength polarization Raman lidar are presented. This study could assist in bridging existing gaps relating to aerosol properties over South Africa, since limited long-term data of this type is available for this region. The observations were performed under the framework of the EUCAARI campaign in Elandsfontein. The multi-wavelength Polly^{XT} Raman lidar system was used to determine vertical profiles of the aerosol optical properties, i.e. extinction and backscatter coefficients, Ångström exponents, lidar ratio and depolarization ratio. The mean microphysical aerosol properties, i.e. effective radius and single scattering albedo ~~was~~were retrieved with an advanced inversion algorithm. Clear differences were observed for the intensive optical properties of atmospheric layers of biomass burning and urban/industrial aerosols. Our results reveal a wide range of optical and microphysical parameters for biomass burning aerosols. This indicates probable mixing of biomass burning aerosols with desert dust particles, as well as the possible continuous influence of urban/industrial aerosol load in the region. The lidar ratio at 355 nm, the lidar ratio at 532 nm, the linear particle depolarization ratio at 355 nm and the extinction-related Ångström exponent from 355 to 532 nm were 52 ± 7 sr; 41 ± 13; 0.9 ± 0.4 % and 2.3 ± 0.5, respectively for urban / industrial aerosols, while these values were 92 ± 10 sr; 75 ± 14; 3.2 ± 1.3 ~~%; 2.~~% and 1.7 ± 0~~ ± 0.4~~.3 respectively for biomass burning aerosols layers. Biomass burning particles are larger and slightly less absorbing compared to urban / industrial aerosols. The particle effective ~~radiuses~~radius were found to be 0.10 ± 0.03 µm, 0.17 ± 0.04 µm and 0.13 ± 0.03 µm for urban/industrial, biomass burning, and mixed ~~biomass burning and desert dust~~ aerosols, respectively, while the single scattering albedo at 532 nm were 0.87 ± 0.06,

49 0.90 ± 0.06, and 0.88 ± 0.07 (at 532 nm), respectively for these three types of
50 aerosols. Our results were within the same range of previously reported values.
51

1. Introduction

Atmospheric aerosols of natural and anthropogenic origin contribute substantially to global climate variability (IPCC, 2013). Currently, the magnitude of the (anthropogenic) aerosol impact on climate causes the largest uncertainty on our knowledge of climate change (Forster et al., 2007). Large uncertainties exist due to the diversity, not only with respect to aerosol particle size, composition, sources and lifetime variation, but also with regard to the spatial and temporal distributions of aerosols. Thus, the impacts of aerosols on climate must be understood and quantified on a regional scale rather than on a global-average basis (Piketh et al., 2002).

High-quality aerosol measurements in the southern hemisphere are rather limited. South Africa is located at the southernmost tip of the African continent, extending from 22^{o} S to 34^{o} S latitude and from 16° E to 32° E longitude. Previous studies have indicated that South Africa is one of the countries in the world that is largely affected by aerosol load, due to various natural and anthropogenic sources (Piketh et al., 2000; Piketh et al., 2002; Formenti et al., 2002, 2003; Campbell et al., 2003; Eck et al., 2003; Freiman and Piketh, 2003; Ichoku et al., 2003; Ross et al., 2003; Winkler et al., 2008; Queface et al., 2011; Tesfaye et al., 2011; Venter et al., 2012; Tiitta et al., 2014). Intensive efforts have been undertaken during recent years to characterize aerosol pollution in South Africa. In general, previous studies pointed at the importance of regional circulation of air masses and seasonal pollutant variation. The optical properties of aerosols have been studied by means of sun photometers (e.g. Queface et al., 2011; Eck et al., 2003), *in situ* data (e.g. Laakso et al., 2012) and satellite observations (e.g. Tesfaye et al., 2011) in these studies, which are based on columnar aerosol optical properties. Ground-based Raman lidars provide vertically resolved information on the distribution and optical properties of aerosols. Giannakaki

et al. (2015) used Raman lidar data obtained over a one year period at Elandsfontein in South Africa (26°15´ S, 29°26´ E, 1745 m above sea level (a.s.l.)) to study the geometrical characteristics, intensive and extensive optical properties of free-tropospheric aerosol layers. In addition to these characteristics that can be determined with lidar data, multi-wavelength Raman lidar measurements can also be used to determine profiles of microphysical particle properties by using inversion algorithms (Twomey, 1977; Veselovskii et al., 2002, Müller et al., 2001). In this study we expand our study of aerosols in South Africa by providing information on the microphysical and optical properties of aerosol layers. This type of aerosol lidar observations are valuable for spaceborne lidars such as CALIPSO (Cloud-Aerosol Lidar and Infrared Pathfinder Satellite Observations) (e.g. Omar et al., 2009), since lidar ratio values for different aerosol types are required for reliable aerosol extinction retrievals. Therefore, this study could be useful for further improving lidar ratio selection-scheme algorithms used in spaceborne lidar missions.

Four long-term ground-based aerosol measurements were carried out at sites in economically growing countries in Asia, Africa and South America within the EUCAARI project (Kulmala et al., 2011), which included Elandsfontein in South Africa. The aim of EUCAARI was to characterize particles in terms of physical, optical and chemical aerosol properties. Here we report lidar observations that were performed at Elandsfontein. In particular, we discuss the optical and microphysical properties of aerosol layers that are caused by biomass burning and urban/industrial activities at the site. We present aerosol lidar ratios, particle linear depolarization ratios and Ångström exponents for biomass burning and urban/industrial aerosol layers measured with a multi-wavelength Raman lidar. The possible effect of desert dust particles on biomass burning aerosol layers in terms of the intensive optical and

microphysical properties is also ~~studied~~addressed. In addition, effective radius and single-scattering albedo are calculated with an advanced inversion algorithm.

The paper is organized as follows: In section 2, the research site, the methodology used for the retrieval of optical and microphysical properties and the aerosol typing are introduced. As a case study, the arrival of a biomass burning aerosol layer over Elandsfontein is discussed in section 3. Section 4 presents the main findings of the optical and microphysical aerosol properties for selected biomass burning ~~and~~, urban/industrial and mixed aerosol layers. We close our contribution with a summary and conclusion in section 5.

2. Location and Methodology

2.1. Measurement site

The measurement site was located on a hill top at Elandsfontein (26°15´ S, 29°26´ E, 1745 m a.s.l.) in the Highveld region of South Africa. The station was located approximately 150 km east of the Johannesburg-Pretoria megacity, which is the largest metropolitan area in South Africa with a population of more than 10 million people (Lourens et al., 2012).

In South Africa, anthropogenic atmospheric emissions are predominantly the product of industrial activities and biomass burning (Ross et al., 2003). South Africa is the most industrialized country of the sub-continent – primarily due to the industrialized Highveld region (Freiman, 2003; Wenig et al., 2003). This region has clusters of industrial complexes and power plants between 25.5° S, 27.5° E and 27.0° S, 30.5° E (Ross et al., 2003), which contributes significantly to aerosol and trace gases pollution (Freiman et al., 2003). Tropospheric NO2 distributions derived with SCIAMACHY (SCanning Imaging Absorption spectroMeter for AtmosphericCHartographY) from August 2002 to March 2012 (Schneider et al., 2015) are presented in Figure 1. The tropospheric NO2 column density of the Highveld region in South Africa is

comparable to that observed over central and northern Europe, eastern North America and Southeast Asia (Lourens et al, 2012).

In addition, emissions from biomass burning (wild fires) contribute significantly to regional emission loads (e.g. Giannakaki et al., 2015). Both, natural phenomena (lightning) and human induced activities are responsible for biomass burning (Edwards et al., 2006). The number of hotspots, with confidence levels between 80-100%, (http://earthdata.nasa.gov/data/nrt-data/firms/active-fire-data), in the latitude range between -40° and 40° and longitude range between -20° and 60° are plotted in Figure 2. The number of hotspots is averaged in terms of 3 months for the year 2010. Wild fires originate in the sub-equatorial central African region and progress southward (Roy et al., 2005). In southern Africa, the fires progress along a north-west to south-east track.

2.2. Description of the lidar system and lidar data processing

The transportable aerosol Raman lidar Polly^{XT} that was operated remotely at Elandsfontain is described by Althausen et al. (2009) and Engelmann et al. (~~2015~~2016). Polly^{XT} works with a Nd:YAG laser emitting at its primary wavelength of 1064 nm, which after frequency doubling and tripling emits at the wavelengths of 532 and 355 nm, respectively. The receiver consists of a Newtonian telescope with a diameter of 300 mm and a field of view of 1 mrad. Photomultiplier tubes (PMT) are used for the detection of the elastically backscattered photons at 355, 532 and 1064 nm, as well as the in-elastically backscattered photons at 387 and 607 nm that correspond to the Raman-shift by nitrogen molecules at 355 and 532 nm, respectively. Additionally, the cross-polarized component at 355 nm is detected and consequently allows for the determination of the linear particle depolarization ratio (also called depolarization ratio). To retrieve the particle depolarization ratio the Rayleigh calibration method was applied within the data analysis under the assumption of pure

Rayleigh depolarization in an aerosol-free height range (Behrendt and Nakamura, 2002). The vertical resolution of the signal profiles is 30 m and the raw data are typically stored as 30 s average values (20 Hz laser frequency). Data were collected on the web page of PollyNet (http://polly.tropos.de) where the "quicklooks" of all measurements are available.

Extinction and backscatter coefficient profiles at 355 and 532 nm, respectively, were obtained with the Raman method (Ansmann et al., 1992~~), while the backscatter coefficient at 1064 nm was determined by using the Klett method (Klett, 1981).~~). To vertically retrieve the backscatter coefficient at 1064 nm we use Fernald-Klett method (Fernald, 1984; Klett, 1981). With this method the particle backscatter coefficient is derived applying a backward iteration starting at a chosen reference height. The method requires independent information on the lidar ratio and on the reference value of the particle backscatter coefficient. The cases analyzed here are night-time measurements and the retrieved backscatter at 1064 nm was also evaluated by the Raman method (Ansmann et al., 1992) using also the signal from the Nitrogen Raman channel at the 607 nm. An overlap correction was applied on the basis of a simple technique proposed by Wandinger and Ansmann (2002). The depolarization ratio, i.e. the ratio of the cross-polarized to the parallel-polarized component of the backscatter coefficient (particles and molecules) at 355 nm was also calculated. The contribution of the molecules can easily be calculated, which then provides the linear particle depolarization ratio (Cairo et al., 1999; Murayama et al., 1999).

The uncertainties affecting the retrieval of extinction and backscatter coefficients, and thus the calculation of lidar ratio and Ångström exponents are mainly due: to the statistical error due to signal detection, the systematic error associated with the estimation of the atmospheric molecular number density from the pressure and

temperature profiles, the systematic error associated with the evaluation of the aerosol scattering wavelength dependence, the systematic error for overlap function, the errors introduced by operation procedure such as signal binning (smoothing) and averaging accumulating lidar returns. The overall relative errors of the lidar-derived aerosol properties range between 5%-15% for the backscatter coefficients, 10%-30% for the extinction coefficients, 20%-40% for the Ångström exponents, 15%-40% for the lidar ratios and approximately 5%-10% for the linear particle depolarization ratio (Hänel et al., 2012~~),~~; Baars et al., 2016, Engelmann et al., 2016). A detailed discussion on the influence of aerosol optical depth errors to Ångström exponent errors can be found in Wagner et al., 2008.

The layer identification was based on the assumption that the optical properties should be relatively stable. This means that within a chosen height layer, the variability of the optical data should be less than the statistical uncertainty of the individual data points. In Table 1 we provide information regarding the elevated layers that were selected for the optical and microphysical aerosol characterization. The characterization of aerosol types will be discussed in section 2.4.

2.3. Retrieval of microphysical properties

Microphysical particle properties are derived with an inversion algorithm that has been developed at the Leibniz Institute for Tropospheric Research. A detailed description of the inversion code is given by Müller et al (1999a, 1999b). A minimum of three backscatter coefficients (355, 532, and 1064 nm) and two extinction coefficients (355 and 532 nm), with measurement errors less than ~~20~~30%, are required as input in order to obtain microphysical results that have reasonably low uncertainties (Müller et al., 2001). The selection of the individual inversion solutions is based on the concept that the back-calculated optical data should agree with the

original data within the limits of the measurement errors, and that a pre-selected discrepancy level, which is an output parameter of the inversion algorithm (Müller et al., 1999a), is not exceeded. The mean particle size in terms of the effective radius is then calculated along with the standard deviation from these selected individual solutions. One also obtains a range of complex refractive indexes by applying this method. The complex refractive index is a wavelength-independent quantity. Therefore, inversion can only provide a wavelength-independent value that represents the entire range of wavelengths from 355 – 1064 nm. The single-scattering albedo can then be calculated from the volume concentration distribution, which is another data product of the inversion algorithm, and the associated mean complex refractive index by means of a Mie scattering algorithm.

Uncertainties associated with the retrievals are in general <30% for effective radius. The real part of the complex refractive index is derived to an accuracy better than ±0.1, while the imaginary part is obtained for its correct order of magnitude if the value is <0.01i (for larger values of the imaginary part the uncertainty is <50%). The single-scattering albedo can be calculated with an accuracy of ±0.05, if uncertainties of the input optical data are on average <10-15%. A detailed error analysis is presented by Müller et al. (1999b, 2001) and Veselovskii et al., (2002, 2004).

2.4. Aerosol classification

The identification of the source of aerosol particles is possible with the synergetic use of in-situ and satellite measurements, as well as ~~utilising~~utilizing model estimations.

The HYSPLIT_4 (Hybrid Single Particle Langrangian Integrated Trajectory) model (Draxler and Hess, 1997) was used to compute backward air mass trajectories employing the kinematic approach and by using the re-analysed National Oceanic and Atmospheric Administration (NOAA) dataset with a resolution of 2.5^{o} x 2.5^{o} (latitude, longitude) as input. Four-day backward trajectories were selected, because they

extend far enough back in time and distance to cover the main source regions suspected to affect the region investigated. The trajectories were calculated for the center of the layer observed and for the time of the lidar measurement ~~(see Table 1).~~.

The number of fire hotspots is given by Moderate Resolution Imaging Spectroradiometer (MODIS) collection-5 active-fire product data (Giglio, L. et al., 2010). The number of hotspots, obtained from MODIS for four days prior to each of the measurements, was superimposed on the trajectory analysis map in order to detect the presence of smoke particles over our site for the cases analyzed.

Trace gases were measured as part of routine air quality monitoring at the site by the national electricity supplier, i.e. Eskom. A Thermo Electron 43C SO_2 analyser and a Thermo Electron 42i NO_x analyser were used to measure SO_2 and NO_x respectively. H_2S was measured with a Thermo Electron 43A SO_2 analyzer with a Thermo Electron 340 converter. 15-minute data were averaged for the extent of measurement time for each of the measurements periods (Table 1). For instances where the combined use of trajectory analysis and fire hotspots did not indicate the presence of biomass burning aerosols we checked whether the measured NO_x, SO_2 or H_2S concentrations were higher than the seasonal mean values of that measured for the entire period of the EUCAARI campaign. These seasonal mean values are presented in Laakso et al. (2012). In addition, when the trace gases concentrations were lower than the mean seasonal values measured during the EUCAARI campaign and biomass-burning activity or desert dust advection were absent, we checked if the daily concentration of the trace gases exceeded the mean critical values.

There were also cases that indicated desert dust aerosol particles in addition to the smoke, which originated either from the Kalahari or the Namibia desert that could have additionally contributed to the aerosol loads. Therefore, the measured aerosol

optical properties determined for these cases were attributed to a mixing state where smoke particles were possible to be mixed ~~state of biomass burning and~~with desert dust aerosols. Additional mixing with urban / industrial aerosols is also possible.

An example of a measurement of biomass burning aerosols is discussed in the subsequent section in order to demonstrate the methodology used to derive the optical and microphysical aerosol properties.

3. Biomass burning aerosols on 1st October 2010 at Elandsfontein, South Africa

In ~~Figure 3, the time height plot of the range corrected signal at 1064 nm is presented for the 1st of October 2010. The figure reveals~~this section we will study a geometrically deep layer that extends up to 2.1 km height above ground level (AGL~~).~~) as observed on the 1st of October 2010. The atmospheric structure, in terms of range corrected signals, is quite stable which indicates similar optical properties throughout the layer~~.~~ (http://polly.tropos.de/?p=bilder&lambda=1064&Jahr=2010&Monat=10&Tag=1&Ort=11#bildanker). High backscatter returns are observed on the day when the measurement is conducted in relation to the previous and the next day~~.~~ (as can be already seen in Figure 4 (a) – light green).

~~In Figure 4, four-day backward trajectories arriving at Elandsfontein at 00:00, 02:00 and 04:00 UTC are presented. The trajectories are computed for arrival heights of 1000 and 1500 m (AGL). The MODIS fire hotspots product is superimposed on the trajectory plot for the four day period. Several~~MODIS fire hotspots product reveal that several fires were active during the period 28th of September 2010 – 1st of October 2010 as shown in Figure ~~4.~~3 (a). In Figure 3 (b), four-day backward trajectories arriving at Elandsfontein on 1st of October 2010 at 00:00 are presented. The

trajectories are computed for arrival heights of the bottom, center and top of the observed layer. The trajectory analysis ~~for the day of the measurement~~along with MODIS fire hotspots reveals that the air masses ~~were either coming from northeasterly or from northwesterly directions. It is therefore~~are highly possible ~~that these air masses carried~~to carry smoke particles ~~to~~at Elandsfontein on the day of the measurement.

In Figure ~~5~~4 the optical lidar profiles are presented. The backscatter and extinction maximum at all three wavelengths ~~was~~were observed within the 0.9 to 1.9 km height range. High values of the lidar ratio of 96 ± 5 sr at 355 nm and 89 ± 5 sr at 532 nm indicate that the smoke particles inside this layer were most likely highly light-absorbing . The Ångström exponent, related to extinction between 355 and 532 nm, was 1.8 ± 0.1, which points to comparably small particles and indicative of fresh smoke~~.~~ (eg. Müller et al., 2005). A constant particle depolarization ratio in the order of 4% is observed at 355 nm throughout the layer. The lack of significant vertical variability of the lidar ratio, the Ångström exponent and the particle depolarization ratio suggests the presence of the same type (biomass burning) of aerosols throughout the layer.

The mean values of extinction (at 355 and 532 nm) and backscatter coefficients (at 355, 532 and 1064 nm) were calculated within the defined layer and were used as input in the inversion algorithm. Effective radius, complex refractive index and single-scattering albedo were calculated with the microphysical inversion code. An effective radius of 0.15 ± 0.02 µm was determined, while the single-scattering albedo was approximately 0.86 at 532 nm that indicates relatively strong-absorbing aerosols.

4. Results and Discussion

We performed optical lidar data analysis, microphysical retrievals and aerosol typing for each of the thirty eight aerosol layers listed in Table 1 in the same way as presented in the example in section 3. Each aerosol layer in Table 1 was classified into one of the three aerosol types, i.e. urban/industrial, biomass burning, and ~~biomass burning~~ mixed ~~with desert dust~~aerosols after thorough visual inspection of the backward trajectories, MODIS hotspots fires products and in-situ aerosol observations, as explained in section 2.4. Table 2 summarizes the mean intensive optical properties (lidar ratio at 355 and 532 nm, depolarization ratio at 355 nm and Ångström exponent related to extinction between 355 and 532 nm) presented together with the associated standard deviations, ranges (minimum and maximum values) and medians.

Figure ~~6~~5 presents the particle lidar ratios at 355 nm versus the extinction-related Ångström exponent for urban/industrial (black), biomass burning (red) aerosol layers as well as for the mixed ~~biomass burning and desert dust~~aerosol layers (green). Different aerosol types occupy different areas in the Ångström-exponent–lidar-ratio plot. Aerosols from urban and industrial activities are on average characterized by larger Ångström exponents than (pure or mixed) biomass burning aerosols. The lidar ratios of biomass burning aerosols are among the highest compared to literature with a mean value of 92 ± 10 sr (e.g. Müller et al., 2007; Nicolae et al, 2013; Amiridis et al., 2009). ~~Anthropogenic~~Urban / Industrial aerosol layers ~~are characterized by~~were found to have lower lidar ~~ratios~~ratio values in the range between 41 and 59 sr at 355 nm. Our results indicate that biomass burning aerosols have lower lidar ratios when they are mixed either with desert dust aerosols or with urban / industrial aerosols. This might be due to the non-spherical shape of desert dust that may have a significant

effect on the lidar ratio. Model calculations show that a deviation from the spherical shape can efficiently increase particle backscattering and thus lower the lidar ratio (Mishchenko et al., 1997), which was also confirmed by Müller et al. (2003). Ångström exponent values of these aerosols ranged from 1.6 to 2.5, with a mean value of 2.0 ± 0.4, which is larger (smaller particles) than the mean value of 1.7 ± 0.3 we observed for 'pure' biomass burning aerosols. The role that hot air close to the surface of the earth plays in generating these dust size distribution is not well understood (Nisantzi et al., 2014). Wind stress close to the surface may be very complex and the sudden release of all the moisture in the hot soil particles may strongly influence the cracking of larger particles into smaller ones and thus lead to a much more complicated size distribution than observed during desert dust outbreaks (Mamouri et al., 2014).

It is evident from Figure ~~6~~5 that Ångström exponent values for the different aerosol types overlap. Therefore, another intensive aerosol property, the linear particle depolarization ratio, which is an indicator of non-spherical particles, was also used. Figure ~~7~~6 shows the lidar ratio at 355 nm versus the depolarization ratio at the same wavelength for the three aerosol types. Different clusters of data pairs can be identified. Lower depolarization ratio values were found for urban/industrial aerosol layers. These aerosol layers are also characterized by lower lidar ratios and thus the data points representing ~~anthropogenic~~urban / industrial pollution occupy the lower left region in Figure ~~6~~5. Significantly larger particle linear depolarization ratios with a mean of 8.3 ± 0.7 % were found for mixed ~~biomass burning and desert dust~~ aerosols. Typical desert dust aerosol depolarization ratios determined in field measurements performed in the northwestern corner of the Sahara ranged from 30 to 35% at 532 nm with a mean value of 31 ± 3% (Freudenthaler et al., 2009). In addition, particle

depolarization ratios ranging between 30 to 35% were also observed for Asian desert dust (Sugimoto et al., 2003, Shimizu et al., 2004, Shin et al., 2015) and desert dust originating from Middle East dust sources (Mamouri et al., 2013). Depolarization ratios of the mixtures of biomass burning aerosols and desert dust particles determined for African biomass burning and dust mixtures ranged between 8 – 26% at 532 nm (Weinzierl et al., 2011, Tesche et al., 2009). Therefore depolarization values reported in this study are at the lower end of these values. This observed difference can be attributed to the different contribution of desert dust particles to the biomass burning plume. However, we should also note that the geometrical shape of the dust particles over the Kalahari desert could be different from the shape of Saharan dust. Also, the possible influence of the backsground urban / industrial aerosols in the mixture should be kept in mind.

A wide range of (lower) depolarization ratios and lidar ratios was found for biomass burning aerosols. This observed variability can be attributed to differences in the chemical composition of the particles that depends on the source region, relative humidity in the atmosphere, the type of fire, or the combined effect of these factors. In addition, the mixing of the biomass burning aerosols with maritime or even urban/industrial background aerosols cannot be excluded as a possible reason for the variability of lidar ratio and depolarization ratio values.

Several statistics of lidar ratios and Ångström exponents for different aerosol types in the world are available for comparison. Figure ~~8~~7 provides some of the general literature with regard to the lidar ratios values at 355 nm and Ångström exponents of urban/industrial and biomass-burning aerosols, as well as for mixtures of biomass burning and desert dust aerosols. To interpret the x-axis of the Figure 7 one should

also look the Table 4. It is evident from Figure ~~8~~7 that intensive aerosol properties are in good agreement with values found from other studies.

The lidar ratio at 355 nm, in particular, shows similar values for ~~anthropogenic~~urban / industrial aerosols in various regions of the world. Ångström exponent values found for urban/industrial particles in this study are at the upper limit of results previously published for this aerosol type, which indicates slightly smaller particles at Elandsfontein that can most probably be ascribed by differences in the emission sources. The depolarization ratio is at the lower limit indicating spherically shaped anthropogenic particles.

The lidar ratio for biomass burning aerosol layers is within the range of previously reported values, although the values tend to be more at the upper limit of the reported values. The Ångström exponents are in very good agreement with previous studies. Müller et al. (2007) studied the growth of free-tropospheric forest fire smoke particles and indicated that the Ångström exponent decreases with the duration of transport. The Ångström exponent values found in this study (1.7 ± 0.3) corresponds to travel times of the biomass burning aerosols between 1 and 3 days, which is confirmed by back-ward trajectory analysis. The characteristics of biomass burning emissions in the subtropical South African region vary according to the type of fuel burned (vegetation type), meteorology and combustion phase (Ross et al., 2003). For example, flaming grass fires produce smoke with more soot compared to smoke emitted from smoldering wood and bush fires (Posfai et al., 2003). Thus differences in the chemical composition of the particles might be one of the reasons for the observed large lidar ratio.

For the ~~biomass burning mixed with desert dust type~~mixed aerosols the lidar ratio values reported here are in very good agreement with previous studies for the mixture

of desert dust and biomass burning aerosols. The contribution of desert dust particles within the observed biomass burning plumes is probably lower, thus resulting in a lower depolarization ratio and larger Ångström exponent than what has been reported in literature for biomass burning mixed with dust as mentioned previously. Groβ et al. (2011) reported neutral wavelength-dependence of the particle depolarization ratios for mixed dust and smoke layers for which Ångström exponents varied between 0.12 and 0.16, while Tesche et al. (2011) reported wavelength-independent linear particle depolarization ratios of 0.12-0.18 at 355, 532 and 710 nm for mixed dust and smoke layers. In that sense our results on particle depolarization ratios at 355 nm are similar to results from these studies reporting linear particle depolarization ratio at 532 nm.

In Figure 9 the effective radius against the Ångström exponent is plotted. In general the plot shows the same features already noted for Figure ~~6~~5. On average the largest aerosols are determined for biomass burning aerosols (red) with an effective radius of 0.17 ± 0.04 µm. Particles from anthropogenic pollution (black) are smaller with a mean effective radius of 0.1 ± 0.03 µm. Our results indicate that the influence of Kalahari desert dust on biomass burning plumes leads to smaller particles compared to pure biomass burning aerosols with a mean effective radius of 0.13 ± 0.03 µm.

Mean microphysical properties i.e. effective radius, single scattering albedo and complex refractive index are listed with their associated standard deviations, ranges (minimum and maximum values) and medians in Table 3. The particles in the biomass-burning aerosol layers show a mean effective radius of 0.17 ± 0.04 µm, which is within the range of values reported in previous studies for biomass burning aerosols. Reid et al. (1998) reported count median diameter values ranging from 0.12 µm for fresh particles to 0.21 µm for aged particles near rain-forest fires in Brazil. Radke et al. (1988) obtain values of approximately 0.22 µm for particles from forest

fires in North America. Wandinger et al. (2002) found larger biomass burning aerosols with an effective radius of approximately 0.25 µm. Effective radii in the range between 0.19 and 0.44 µm were found for biomass burning aerosol layers resulting from long-range transport across Romania (Nicolae et al., 2013). Müller et al, (2007) presented values ranging between 0.13 and 0.15 nm for plumes ageing between one to three days.

The three types of aerosols cover a wide range of single-scattering albedo values as shown in Table 3. The mean single-scattering albedo for biomass burning aerosol is 0.90 ± 0.06 (at 532 nm). Lower single scattering albedos are reported in literature for fresh biomass burning particles in Europe. Nicolae et al. (2013) reported a value of 0.78 ± 0.02, while Reid et al. (1998) found that single scattering albedo ranges between 0.74 and 0.77 for fresh smoke. Previous studies show that aged biomass burning layers are characterized by larger single scattering albedos. For example, Murayama et al. (2004) found a value of 0.95 ± 0.06 at 532 nm, while Noh et al. (2009) reported single scattering albedos of 0.92 at the same wavelength. Therefore our results indicate moderately absorbing particles resulting from fresh or medium aged (less than 3 days) biomass burning aerosols.

For the ~~biomass burning~~ mixed aerosols ~~that are mixed with desert dust particles~~ we determined lower mean scattering-albedos of 0.88 ± 0.07, which is slightly higher than the mean single-scattering albedo of 0.87 ± 0.06 determined for urban/industrial aerosol layers. Laakso et al. (2012) reported values of 0.84 ± 0.08 (637 nm) at ground level at Elandsfontein, South Africa. Quaface et al. (2011) determined significantly larger values of 0.91 and 0.89 at 440 nm and 670 nm, respectively, from AERONET data collected at Skukuza in South Africa. Our results indicate that elevated

anthropogenic aerosol layers from urban and industrial activities are characterized by stronger light-absorption.

Complex refractive indexes are also reported in Table 3. Real parts of the complex refractive index of these particles are mostly > 1.5, while imaginary parts vary from 0.007i to 0.04i. Lower real parts of the refractive index are found for biomass burning aerosols compared to the urban/industrial particulates with values ranging from 1.35 to 1.57. The imaginary parts of the refractive index of biomass burning aerosol layers are < 0.03i (with the exception of one case that shows an imaginary refractive index of 0.046i). A large variation of refractive indices for the real and imaginary parts is observed for ~~biomass burning aerosols~~ mixed ~~with desert dust~~ aerosols. This might allude to the different levels of contribution of Kalahari desert dust to biomass burning aerosol layers.

5. Summary and Conclusions

Thirty eight aerosol layers of urban/industrial, biomass burning, and mixed ~~biomass burning and desert dust~~ aerosols were studied with regard to their optical and microphysical properties at Elandsfontein, South Africa. The combination of Raman lidar observations with backward trajectory analysis, satellite fire observations and *in situ* data allowed for source identification of the elevated aerosol layers. Measurements of the lidar ratios and depolarization ratios are presented in order to assist in the separation of anthropogenic, biomass burning, and mixtures of ~~biomass burning with desert dust particles~~aerosols.

A wide range of optical (lidar ratio and depolarization ratio) and microphysical (single scattering albedo, complex refractive index) properties was determined for biomass burning aerosols, indicating differences in chemical composition. Aerosols from

urban and industrial activities are on average characterized by larger Ångström exponents than (pure or mixed) biomass burning aerosols. Lidar ratios for biomass burning aerosols are among the highest found in literature with a mean value of 92 ± 10 sr, while the anthropogenic aerosols are characterized by lower lidar ratios in the range between 41 and 59 sr at 355 nm. Ångström exponents were found to be similar for all types of aerosol types under study, with slightly larger values determined for anthropogenic aerosols. Mean effective radii of 0.17 ± 0.04 μm and 0.1 ± 0.03 μm were calculated for biomass burning and ~~anthropogenic~~urban / industrial aerosols, respectively. We have also shown that in certain instances biomass burning aerosols may contain a small amount of desert dust particles resulting in higher depolarization ratios and lower lidar ratios than the values reported for pure biomass burning aerosols. Moderately absorbing particles were found for biomass burning layers with a mean single scattering albedo of 0.9 ± 0.06. ~~Biomass burning~~Mixed aerosols ~~mixed with desert dust particles,~~ were found more absorbing with a mean single-scattering albedo of 0.88 ± 0.07. A slightly lower mean single-scattering albedo of 0.87 ± 0.06 was found for urban~~/~~ / industrial aerosol layers. However, this value was larger than the values reported for the same site from ground-based in-situ measurements. Our optical and microphysical results for the analyzed aerosol types agreed very well with similar studies reported in literature.

Ground-based lidar networks provide information on the vertical and horizontal distribution of optical aerosol properties in a systematic and statistically significant manner. Different lidar networks that are globally distributed observe aerosols in Europe, South America, Asia and North America. The analysis of lidar measurements presented here could assist in bridging existing gaps with regard to our knowledge of the vertical distribution of optical and microphysical aerosols in the South African

503 atmosphere, since limited long-term data of this nature is available for this region. Our
504 results could also be useful for lidar ratio selection schemes needed for elastic-
505 backscatter lidars. In that sense our findings could be used in advancing lidar
506 algorithms used for present and/or future satellite lidar missions.
507
508
509 **ACKNOWLEDGMENTS**

510 This work has been partly supported by the European Commission 6th Framework
511 program under the EUCAARI project (contract no. 036833-2). Elina Giannakaki
512 acknowledges the support of the Academy of Finland (project no. 270108). The
513 authors acknowledge the staff of the North-West University for valuable assistance
514 and routine maintenance of the lidar. We also acknowledge Eskom and Sasol for their
515 logistical support for measurements at Elandsfontein.
516

REFERENCES

Alados Arboledas, L., Müller, D., Guerrero Rascado, J. L., Navas Guzmán, F., Pérez Ramírez, D., and Olmo, F. J.:, Optical and microphysical properties of fresh biomass burning aerosol retrieved by Raman lidar, and star and sun-photometry, Geophys. Res. Lett., 38, L01807, doi:10.1029/2010GL045999, 2011.

Althausen, D., Engelmann, R., Baars, H., Heese, B., Ansmann, A., Müller, D., and Komppula, M.: Portable Raman Lidar Polly^{XT} for Automated Profiling of Aerosol Backscatter, Extinction, and Depolarization, J. Atmos. Ocean. Technol., 26, 2366-2378, doi: 10.1175/2009jtecha1304.1, 2009.

Amiridis, V., Balis, D. S., Giannakaki, E., Stohl, A., Kazadzis, S., Koukouli, M. E., and Zanis, P.: Optical characteristics of biomass burning aerosols over Southeastern Europe determined from UV-Raman lidar measurements, Atmos. Chem. Phys., 9, 2431-2440, doi:10.5194/acp-9-2431-2009, 2009.

Ansmann, A., Wandinger, U., Riebesell, M., Weitkamp, C., and Michaelis, W.: Independent measurement of extinction and backscatter profiles in cirrus clouds by using a combined Raman elastic-backscatter lidar, Appl. Optics, 31, 7113-7131, doi: 10.1364/AO.31.007113,1992.

Ansmann, A., Engelmann, R., Althausen, D., Wandinger, U., hu, M., Zhang, Y., and He, Q.: High aerosol load over the Pearl River Delta, China, observed with Raman lidar and Sun photometer, Geophys. Res. Lett., 32, L13815, doi: 10.1029/2005GL023094, 2005.

Ansmann A., Baars, H., Tesche, M., Müller, D., Althausen, D., Engelmann, R., Pauliquevis, T., and Artaxo, P.: Dust and smoke transport from Africa to South America : Lidar profiling over Cape Verde and the Amazon rainforest, Geophys. Res. Lett., 36, L11802, doi:10.1029/2009GL037923, 2009.

Baars, H., Ansmann, A., Althausen, D., Engelmann, R., Artaxo, P., Pauliquevis, T., and Souza, R.: Further evidence for significant smoke transport from Africa to Amazonia, Geophys. Res. Lett., 38, L20 802, doi: 10.1029/2011GL049200, 2011.

545 Baars, H., Ansmann, A., Althausen, D., Engelmann, R., Heese, B., Müller, D., Artaxo,
546 P., Paixao, M., Pauliquevis, T., and Souza, R.: Aerosol profiling with lidar in Amazon
547 Basin during the wet and dry season, J. Geophys. Res., 117, D21201, doi:
548 10.1029/2012JD018338, 2012.

549 Baars, H., Kanitz, T., Engelmann, R., Althausen, D., Heese, B., Komppula, M.,
550 Preißler, J., Tesche, M., Ansmann, A., Wandinger, U., Lim, J.-H., Ahn, J. Y.,
551 Stachlewska, I. S., Amiridis, V., Marinou, E., Seifert, P., Hofer, J., Skupin, A.,
552 Schneider, F., Bohlmann, S., Foth, A., Bley, S., Pfüller, A., Giannakaki, E.,
553 Lihavainen, H., Viisanen, Y., Hooda, R. K., Pereira, S. N., Bortoli, D., Wagner, F.,
554 Mattis, I., Janicka, L., Markowicz, K. M., Achtert, P., Artaxo, P., Pauliquevis, T.,
555 Souza, R. A. F., Sharma, V. P., van Zyl, P. G., Beukes, J. P., Sun, J., Rohwer, E. G.,
556 Deng, R., Mamouri, R.-E., and Zamorano, F.: An overview of the first decade of
557 PollyNET: an emerging network of automated Raman-polarization lidars for
558 continuous aerosol profiling, Atmos. Chem. Phys., 16, 5111-5137, doi:10.5194/acp-
559 16-5111-2016, 2016.

560 Balis, D.S., Amiridis, V., Zerefos, C., Gerasopoulos, E., Andreae, M., Zanis, P.,
561 Kazantzidis, A., Kazadzis, S. and Papayannis A.: Raman lidar and Sun photometric
562 measurements of aerosol optical properties over Thessaloniki, Greece during a
563 biomass burning episode 2003, Atmos. Environ., 37(32), 4529–4538,
564 doi:10.1016/S1352-2310(03)00581-8, 2003.

565 Burton, S.P., Ferrare, R.A., Hostetler, C.A., Hair, J.W., Rogers, R.R, Obland, M.D.,
566 Butler, C.F., Cook, A.I., Harper, D.B., and Froyd, K.D.: Aerosol classification using
567 airborne High Spectral Resolution Lidar measurements – methodology and examples,
568 Atmos. Meas. Tech., 5, 73-98, doi: 10.5194/amt-5-73-2012, 2012.

569 Burton, S.P., Ferrare, R.A., Vaughan, M.A., Omar, A.H., Rogers, R.R., Hostetler,
570 C.A., and Hair, J.W.: Aerosol classification from airborne HSRL and comparisons
571 with the CALIPSO vertical feature mask, Atmos. Meas. Tech., 6, 1397-1412,
572 doi:10.5194/amt-6-1397-2013, 2013.

573 Cairo, F., Di Donfrancesco, G., Adriani, A., Pulvirenti, L. and Fierli, F.: Comparison
574 of various linear depolarization parameters measured by lidar, Appl. Opt. 38, 4425-
575 4432, doi: 10.1364/AO.38.004425,1999.

576 Campbell, J. R., Welton, E. J., Spinhirne, J. D., Ji, Q., Tsay, S. C., Piketh, S. J.,
577 Barenbrug, M., and Holben, B. N.: Micropulse lidar observations of tropospheric
578 aerosols over northeastern South Africa during the ARREX and SAFARI 2000 dry
579 season experiments, J. Geophys. Res., 108, D13, 8497, doi: 10.1029/2002jd002563,
580 2003.

581 Draxler, R. R. and Hess, G. D.: Description of the HYSPLIT 4 modeling system,
582 NOAA Tech Memo, ERL ARL-224, 24, NOAA, Silver Spring, Md., 1997.

583 Eck, T. F., Holben, B. N., Ward, D. E., Mukelabai, M. M., Dubovik, O., Smirnov, A.,
584 Schafer, J. S., Hsu, N. C., Piketh, S. J., Queface, A., Le Roux, J., Swap, R. J., and
585 Slutsker, I.: Variability of biomass burning aerosol optical characteristics in southern
586 Africa during the SAFARI 2000 dry season campaign and a comparison of single
587 scattering albedo estimates from radiometric measurements, J. Geophys. Res., 108,
588 D13, 8477, doi: 10.1029/2002jd002321, 2003.

589 Edwards, D.P., Emmons, L.K., Gille, J.C., Chu, A., Attie, Giglio, L., Wood, S.W.,
590 Haywood, J., Deeter, M.N., Massie, S.T., Ziskin, D.C., and Drummond, J.R.:
591 Satellite-onserved pollution from Southern Hemisphere biomass burning, J. Geophys.
592 Res., 111, doi: 10.1029/2005JD006655, 2006.

593 Engelmann, R., Kanitz, T., Baars, H., Heese, B., Althausen, D., Skupin, A.,
594 Wandinger, U., Komppula, M., Stachlewska, I. S., Amiridis, V., Marinou, E., Mattis,
595 I., Linné, H., and Ansmann, A.: ~~EARLINET~~The automated multiwavelength Raman
596 ~~Lidar~~polarization and water-vapor lidar PollyXT: the neXT generation, Atmos. Meas.
597 Tech~~. Discuss., 8, 7737–7780~~., 9, 1767–1784, doi:10.5194/~~amtd-8-7737-2015,~~
598 ~~2015~~amt-9-1767-2016, 2016.

599 Formenti, P., Elbert, W., Maenhaut, W., Haywood, J., Osborne, S., and Andreae, M.
600 O.: Inorganic and carbonaceous aerosols during the Southern African Regional
601 Science Initiative (SAFARI 2000) experiment: Chemical characteristics, physical
602 properties, and emission data for smoke from African biomass burning, J. Geophys.
603 Res., 108, D13, 16, doi: 10.1029/2002jd002408, 2003.

604 Formenti, P., Winkler, H., Fourie, P., Piketh, S., Makgopa, B., Helas, G., and
605 Andreae, M. O.: Aerosol optical depth over a remote semi-arid region of South Africa

from spectral measurements of the daytime solar extinction and the nighttime stellar extinction, Atmos. Res., 62, 11-32, doi: 10.1016/s0169-8095(02)00021-2, 2002.

Forster, P., Ramaswamy, V., Artaxo, P., Berntsen, T., Betts, R., Fahey, D., Haywood, J., Lean, J., Lowe, D., Myhre, G., Nganga, J., Prinn, R., Raga, G., Schulz, M. and Dorland, R. V.: Changes in atmospheric constituents and in radiative forcing. Climate Change 2007: The Physical Science Basis. Contribution of Working Group I to the Fourth Assessment Report of the Intergovernmental Panel on Climate Change, Cambridge Univ. Press, Cambridge, UK and New York, NY, USA, 129–234, 2007.

Freiman, M. T., and Piketh, S. J.: Air transport into and out of the industrial Highveld region of South Africa, J. Appl. Meteorol., 42, doi: 10.1175/1520-0450(2003)042<0994:ATIAOO>2.0.CO;2, 994-1002, 2003.

Freudenthaler, V., Esselborn, M., Wiegner, M., Heese, B., Tesche, M., Ansmann, A., Müller, D., Althausen, D., Wirth, M., Fix, A., Ehret, G., Knippertz, P., Toledano, C., Gasteiger, J., Garhammer, M., and Seefeldner, M.: Depolarization ratio pro- filing at several wavelengths in pure Saharan dust during SAMUM 2006, Tellus B, 61, 165–179, doi:10.1111/j.1600- 0889.2008.00396.x, 2009.

Giannakaki, E., Balis, D. S., Amiridis, V., and Zerefos, C.: Optical properties of different aerosol types: seven years of combined Raman-elastic backscatter lidar measurements in Thessaloniki, Greece, Atmos. Meas. Tech., 3, 569-578, doi: 10.5194/amt-3-569-2010, 2010.

Giannakaki, E., Pfüller, A., Korhonen, K., Mielonen, T., Laakso, L., Vakkari, V., Baars, H., Engelmann, R., Beukes, J.P., Van Zyl, P.G., Josipovic, M., Tiitta, P., Chiloane, K., Piketh, S., Lihavainen, H., Lehtinen, K.E.J., and Komppula, M.: One year of Raman lidar observations of free-tropospheric aerosol layers over South Africa, Atmos. Chem. Phys., 15, 5429-5442, doi: 10.5194/acp-15-5429-2015, 2015.

Giglio, L., Randerson, J. T., van der Werf, G.R., Kasibhatla, P. S., Collatz, G. J., Morton, D. C., and DeFries, R. S.: Assessing variability and long-term trends in burned area by merging multiple satellite fire products, Biogeosciences, 7, 1171-1186, doi: 10.5194/bg-7-1171-2010, 2010.

635 Groß, S., Esselborn, M., Weinzierl, B., Wirth, M., Fix, A., and Petzold, A.: Aerosol
636 classification by airborne high spectral resolution lidar observations, Atmos. Chem.
637 Phys., 13, 2487-2505, doi: 10.5194/acp-13-2487-2013, 2013.

638 Groß, S, Tesche, M., Freudenthaler, V., Toledano, C., Wiegner, M., Ansmann, A.,
639 Althausen, D., and Seefeldner, M.: Characterization of Saharan dust, marine aerosols
640 and mixtures of biomass-burning aerosols and dust by means of multi-wavelength
641 depolarization and Raman lidar measurements during SAMUM 2, Tellus B, 63,706-
642 724, doi: 10.1111/j.1600-08892011.00556.x, 2011.

643 Hänel, A., Baars, H., Althausen, D., Ansmann, A., Engelmann, R., and Sun, Y. J.:
644 One-year aerosol profiling with EUCAARI Raman lidar at Shangdianzi GAW station:
645 Beijing plume and seasonal variation, J. Geophys. Res., 117, D13201,
646 doi:10.1029/2012JD017577, 2012.

647 Heese, B. :., Althausen, D., Baars, H., Bohlmann, S., and Deng, R.: Aerosol properties
648 over Southeastern chinaChina from multiwavelength ramanRaman and depolarization
649 lidar measurementsmeasurents, in: Reviewed and Revised Papers of 27th ILRC,
650 International Laser and Radar Conference, 5–10 July 10 2015, New York, USA, 2015.

651 Ichoku, C., Remer, L. A., Kaufman, Y. J., Levy, R., Chu, D. A., Tanre, D., and
652 Holben, B. N.: MODIS observation of aerosols and estimation of aerosol radiative
653 forcing over southern Africa during SAFARI 2000, J. Geophys. Res., 108, 13, doi:
654 10.1029/2002jd002366, 2003.

655 Illingworth, A.J., Barker, H.W., Beljaars, A., Ceccaldi, M., Chepfer, H., Cole, J.,
656 Delanoë, J., Domenech, C., Donovan, D.,P., Fukuda, S., Hirakata, M., Hogan, R.J.,
657 Huenerbein, A., Kollias, P., Kubota, T., Nakajima, T., Nakajima, T.Y., Nishizawa, T.,
658 Ohno, Y., Okamoto, H., Oki, R., Sato, K., Satoh, M., Shephard, M., Wandinger, U.,
659 Wehr, T., and Van Zadelhoff, G.-J.: THE EARTHCARE SATELLITE: The next step
660 forward in global measurements of clouds, aerosols, precipitation and radiation,
661 Bulletin of the American Meteorological Society (BAMS),
662 doi: http://dx.doi.org/10.1175/BAMS-D-12-00227.1, 2015.

663 IPCC: The Physical Science Basis, Contribution of Working Group I to the Fifth
664 Assessment Report of the Intergovernmental Panel on Climate Change, edited by :

Formatted: English (U.S.)
Formatted: English (U.S.)
Formatted: English (U.S.)
Formatted: English (U.S.)
Formatted: English (U.S.)
Formatted: English (U.S.)
Formatted: English (U.S.)
Formatted: English (U.S.)
Formatted: English (U.S.)

Stocker, T. F., Qin, D., Plattner, G.-K, Tignor, M., Allen, S. K., Boschung, J., Nauels, A., Xia, Y., Bex, V., and Midgley, P. M., Cambridge University Press, Cambridge, United Kingdom and New York, NY, USA, 2013.

Kanitz, T., Ansmann, A., Engelmann, R., and Althausen, D.: North-south cross sections of the vertical aerosol distribution over the Atlantic Ocean from multiwavelength Raman/polarization lidar during Polarstern cruises, J. Geophys. Res.,118, 2643-2655, doi: 10.1002/jgrd.50273, 2013.

Kanitz, T., Engelmann, R., Heinold, B., Baars, H., Skupin, A., and Ansmann A.: Tracking the Saharan Air Layer with shipborne lidar across the tropical Atlantic, Geophys. Res. Lett., 41, 1044-1050, doi: 10.1002/20133GL058780, http://dx.doi.org/10.1002/2013GL058780, 2014.

Klett, ~~1981.~~J.D.: Stable analytical inversion solution for processing lidar returns, Appl. Optics, 20, 211-220, doi: 10.1364/AO.20.000211, 1981.

Komppula, M., Mielonen, T., Arola, A., Korhonen, K., Lihavainen, H., Hyvärinen, A. P., Baars, H., Engelmann, R., Althausen, D., Ansmann, A., Müller, D., Panwar, T. S., Hooda, R. K., Sharma, V. P., Kerminen, V. M., Lehtinen, K. E. J., and Viisanen, Y.: Technical Note: One year of Raman-lidar measurements in Gual Pahari EUCAARI site close to New Delhi in India - Seasonal characteristics of the aerosol vertical structure, Atmos. Chem. Phys., 12, 4513-4524, doi: 10.5194/acp-12-4513-2012, 2012.

Kulmala, M., et al., General overview: European Integrated project on Aerosol Cloud Climate and Air Quality interactions (EUCAARI) – integrating aerosol research from nano to global scales, Atmos. Chem. Phys., 11, 13061-13143, doi: 10.5194/acp-11-13061-2011, 2011.

Laakso, L., Vakkari, V., Virkkula, A., Laakso, H., Backman, J., Kulmala, M., Beukes, J. P., van Zyl, P. G., Tiitta, P., Josipovic, M., Pienaar, J. J., Chiloane, K., Gilardoni, S., Vignati, E., Wiedensohler, A., Tuch, T., Birmili, W., Piketh, S., Collett, K., Fourie, G. D., Komppula, M., Lihavainen, H., de Leeuw, G., and Kerminen, V. M.: South African EUCAARI measurements: seasonal variation of trace gases and aerosol optical properties, Atmos. Chem. Phys., 12, 1847-1864, doi: 10.5194/acp-12-1847-2012, 2012.

Lourens, A. S. M., Butler, T. M., Beukes, J. P., van Zyl, P. G., Beirle, S., Wagner, T. K., Heue, K. P., Pienaar, J. J., Fourie, G. D., and Lawrence, M. G.: Re-evaluating the NO2 hotspot over the South African Highveld, S. Afr. J. Sci., 108, doi: 54-59, 10.4102/sajs.v108i11/12.1146, 2012.

Mamouri, R. E., Ansmann, A., Nisantzi, A., Kokkalis, P., Schwarz, A. and Hadjimitsis D.: Low Arabian dust extinction-to-backscatter ratio, Geophys. Res. Lett., 40, 4762-4766, doi:10.1002/grl.50898, 2013.

Mamouri, R.E. and Ansmann, A.: Fine and coarse dust separation with polarization lidar, Atmos. Meas. Tech., 7, 3717-3735, doi:10.5194/amt-7-3717-2014, 2014.

Mishchenko, M., Travis, L.D., Kahn, R.A. and West, R.A.: Modeling phase functions for dustlike tropospheric aerosols using a shape mixture of randomly oriented polydisperse spheroids, J. Geophys. Res., 102, 16831-16847, 1997.

Müller, D., Wandinger, U. and Ansmann, A.: Microphysical particle parameters from extinction and backscatter lidar data by inversion with regularization: theory, Appl. Opt. 38, 2346–2357, 1999a.

Müller, D., Wandinger, U. and Ansmann, A.: Microphysical particle parameters from extinction and backscatter lidar data by inversion with regularization: simulation, Appl. Opt. 38, 2358–2368, 1999b.

Müller, D., Wandinger, U., Althausen, D., and Fiebig, M.: Comprehensive particle characterization from three-wavelength Raman-lidar observations, Appl. Opt., 40, 4863–4869, doi:10.1364/AO.40.004863, 2001.

Müller, D., Mattis, I., Wandinger, U., Ansmann, A., Althausen, D., Dubovik, O., Eckhardt, S., Stohl, A.: Saharan dust over a central European EARLINET-AERONET site: ~~Combined~~combined observations with Raman lidar and Sun photometer, J. Geophys. Res., 108, ~~D12, 17 p.,~~doi:10.1029/2002JD002918, 4345, 2003.

Müller, D., Mattis, I., Wandinger, U., Ansmann, A., Althausen, D. and Stohl, A.: Raman lidar observations of aged Siberian and Canadian forest fire smoke in the free troposphere over Germany in 2003: Microphysical particle characterization, J.

723 Geophys. ~~Res., 110, D17201, doi:10.1029/2004JD005756~~Res., 110, D17201,
724 doi:10.1029/2004JD005756, 2005.

725 Müller, D., Ansmann, A., Mattis, I., Tesche, M., Wandinger, U., Althausen, D., and
726 Pissani, G.: Aerosol-type dependent lidar raios observed with Raman lidar, J.
727 Geophys. Res., 12, D16202, doi:10.1029/2006JD008292, 2007.

728 Murayama, T., Okamoto, H., Kaneyasu, N., Kamataki, H., Miura, K., Application of
729 lidar depolarization measurement in the atmospheric boundary layer : Effects of dust
730 and sea-salt particles, J. Geophys. Res., 104, 31781-31792, doi:
731 10.1029/1999JD900503, 1999.

732 Murayama, T., Masonis, S. J., Redemann, J., Aderson, T. L., Schmid, B., Living J. M,
733 Russell, P. B., Huebert, B., Howell, S. G., McNaughton, C. S., Clarke, A., Abo, M.,
734 Shimizu, A., Sugimoto, N., Yabuki, M., Kuze, H., Fukagawa, S., Maxwell-Meier K.,
735 Weber, R. J., Orsini, D.A., Blomquist, B., Bandy, A., and Thornton, D.: An
736 intercomparison of lidar-derived aerosol optical properties with airborne
737 measurements near Toko during ACE-Asia, J. Geophys. Res., 108, D23, 8651, doi:
738 10.1029/2002JD003259, 2003.

739 Murayama, T., Müller, D., Wada, K., Shimizu, A., Sekigushi, M., and Tsukamato, T.:
740 Characterization of Asian dust and Siberian smoke with multi-wavelength Raman
741 lidar over Tokyo, Japan in spring 2003, Geophys. Res. Lett., 31, L23103, doi:
742 10.1029/2004GL021105, 2004.

743 Nicolae, D., Nemuc, A., Müller, D., Talianu, C., Vasilescu, J., Belegante L., and
744 Kolgotin, A.: Characterization of fresh and aged biomass burning events using
745 multiwavelength Raman lidar and mass spectrometry, J. Geophys. Res., 118, 2956-
746 2965, doi:10.1002/jgrd.50324, 2013.

747 Nisantzi, A., Mamouri, R.E., Ansmann, A., and Hadjimitsis, D.: Injection of mineral
748 dust into the free troposphere during fire events observed with polarization lidar at
749 Limassol, Cyprus, Atmos. Chem. Phys., 14, 12155-12165, doi: 10.5194/acp-14-
750 12155-2014, 2014.

751 Noh, Y. M., Müller, D., Shin, D. H., Lee, H. L., Jung, J. S., Lee, K. H., Cribb, M., Li,
752 Z., and Kim Y. J.: Optical and microphysical properties of severe haze and smoke
753 aerosol measured by integrated remote sensing techniques in Gwangju, Korea, Atmos.
754 Environ., 43, 879–888, doi:10.1016/j.atmosenv.2008.10.058, 2009.

755 Omar, A., Winker, D., Vaughan, M., Hu, Y., Trepte, C., Ferrare, R., Lee, K.,
756 Hostetler, C., Kittaka, C., Rogers, R., Kuehn, R., and Liu, Z.: The CALIPSO
757 Automated Aerosol Classification and Lidar Ratio Selection Algorithm. J. Atmos.
758 Oceanic Technol., 26, doi: http://dx.doi.org/10.1175/2009JTECHA1231.1 1994–
759 2014, 2009.

760 Piketh, S. J., Swap, R. J., Maenhaut, W., Annegarn, H. J., and Formenti, P.: Chemical
761 evidence of long-range atmospheric transport over southern Africa, J. Geophys. Res.,
762 107, D24, 4817, doi: 10.1029/2002jd002056, 2002.

763 Piketh, S. J., Tyson, P. D., and Steffen, W.: Aeolian transport from southern Africa
764 and iron fertilization of marine biota in the South Indian Ocean, S. Afr. J. Sci., 96,
765 244-246, 2000.

766 Pósfai, M., Simonics, R., Li, J., Hobbs, P. V., and Buseck, P. R.: Individual aerosol
767 particles from biomass burning in southern Africa: 1. Compositions and size
768 distributions of carbonaceous particles, J. Geophys. Res., 108, 2156-2202, doi:
769 10.1029/2002JD002291, 2003.

770 Preiβler, J., Bravo-Aranda, J. Wagner, F., Granados-MuñOZ, M. J., Navas-Guzmán,
771 F., Guerrero-Rascado, J.L., Lyamani, H., and Alados-Arboledas, L.,: Optical
772 properties of free tropospheric aerosol from multi-wavelength Raman lidars over the
773 southern Iberian Peninsula, in: Proceedings of the 9th International Symposium on
774 Tropospheric Profinling, l'Aquila, Italy (September 3-7, 2012), doi:ISBN 978-90-
775 815839-4-7, 2012.

776 Preiβler, J., Wagner, F., Guerrero-Rascado, J.L., and Silva, A.M.: Two years of free-
777 tropospheric aerosol layers observed over Portugal by lidar, J. Geophys. Res., 118,
778 3676-3686, doi:10.1002/jgrd.50350, 2013.

779 Queface, A. J., Piketh, S. J., Eck, T. F., Tsay, S. C., and Mavume, A. F.: Climatology
780 of aerosol optical properties in Southern Africa, Atmos. Environ., 45, 2910-2921, doi:
781 10.1016/j.atmosenv.2011.01.056, 2011.

782 Radke, L.F., Heggs, D.A., Lyons, H., Brook, C.A., Hobbs, P.V., Weiss, R., and
783 Rasmussen, R.: Airborne measurements on smoke from biomass burning, in Aerosols
784 and Climate, edited by Hobbs, P.V. and McCormick, M. P., ~~pp. 411-422,~~ Deepak, A.,
785 Hampton, VA, USA, 411–422, 1998.

786 Reid, J.S., Koppmann, R., Eck, T.F, and Eleuterio, D. P. : A review of biomass
787 burning emissions, part II. Intensive physical properties of biomass burning particles,
788 Atmos. Chem. Phys., 5, 799-825, doi: 10.5194/acp-5-799-2005, 2005.

789 Reid, J. S., and P. V. Hobbs: Physical and optical properties of smoke from individual
790 biomass fires in Brazil, J. Geophys. Res., 103, 32013–32031, doi:
791 10.1029/98JD00159, 1998.

792 Ross, K. E., Piketh, S. J., Bruintjes, R. T., Burger, R. P., Swap, R. J., and Annegarn,
793 H. J.: Spatial and seasonal variations in CCN distribution and the aerosol-CCN
794 relationship over southern Africa, J. Geophys. Res., 108, D13, 8481, doi:
795 10.1029/2002JD002384, 2003.

796 Roy, D.P., Frost, P.G.H., Justice, C.O., Landmann, T., Le Roux, J.L., Gumbo, K.,
797 Makungwa, S., Dunham, K., du Toit, R., Mhwandagara, K., Zacarias, A., Tacheba,
798 B., Dube, O.P., Pereira, J.M.C., Mushove, P., Morisette, J.T., Santhana-Vannan S.K.,
799 and Davies, D.: The Southern Africa Fire Network (SAFnet) reigional burned-area
800 product-validation protocol, Int. J. Remote Sens., 26, 4265-4292, 2005

801 Roy, D. P., Boschetti, L., Justice, C. O. and Ju, J.: The collection 5 MODIS burned
802 area product – Global evaluation by comparison with the MODIS active fire product,
803 Remote Sens. Environ., 112, 3960-3707, doi: 10.1016/j.rse.2008.05.013, 2008.

804 Schneider, P., Lahoz, W. A., and van der A, R.: Recent satellite-based trends of
805 tropospheric nitrogen dioxide over large urban agglomerations worldwide, Atmos.
806 Chem. Phys., 15, 1205–1220, 2015.

807 Shimizu, A., Sugimoto, N., Matsui, I., Arao, K., Uno, I., Murayama, T., Kagawa, N.,
808 Aoki, K., Uchiyama, A., and Yamazaki, A.: Continuous observations of Asian dust
809 and other aerosols by polarization lidars in China and Japan during ACE-Asia, J.
810 Geophys. Res., 109, D19S17, doi:10.1029/2002JD003253, 2004.

811 Shin, S.-K., Müller, D., Lee, C., Lee, K. H., Shin, D., Kim, Y. J. and Noh, Y. M.:
812 Vertical variation of optical properties of mixed Asian dust/pollution plumes
813 according to pathway of air mass transport over East Asia, Atmos. Chem. Phys., 15,
814 6707-6720, doi:10.5194/acp-15-6707-2015, 2015.

815 Sugimoto, N., Uno, I., Nishikawa, M., Shimizu, A., Matsui, I., Dong, X., Chen, Y.,
816 and Quan, H.: Record heavy Asian dust in Beijing in 2002: Observations and model
817 analysis of recent events, Geophys. Res. Lett., 30, 1640, doi:10.1029/2002GL016349,
818 2003.

819 Tesche, M., Ansmann, A., Müller, D., Althausen, D., Engelmann, R., Freudenthaler,
820 V., and Groß, S.: Vertically resolved separation of dust and smoke over Cape Verde
821 using multiwavelength Raman and polarization lidars during Saharan Mineral Dust
822 Experiment 2008, J. Geophys. Res., 114, D13202, doi:10.1029/2009JD011862, 2009.

823 Tesche, M., Gross, S., Ansmann, A., Müller, D., Althausen, D., Freudenthaler, V., and
824 Esselborn, M.: Profiling of Saharan dust and biomass-burning smoke with
825 multiwavelength polarization Raman lidar at Cape Verde, Tellus B, 63, available at:
826 http://www.tellusb.net/index.php/tellusb/article/view/16360, (last access: 14
827 December 2015), 2011.

828 Tesfaye, M., Sivakumar, V., Botai, J., and Tsidu, G. M.: Aerosol climatology over
829 South Africa based on 10 years of Multiangle Imaging Spectroradiometer (MISR)
830 data, J. Geophys. Res., 116, D20216, doi: 10.1029/2011jd016023, 2011.

831 Tiitta, P., Vakkari, V., Croteau, P., Beukes, J. P., van Zyl, P. G., Josipovic, M.,
832 Venter, A. D., Jaars, K., Pienaar, J. J., Ng, N. L., Canagaratna, M. R., Jayne, J. T.,
833 Kerminen, V.-M., Kokkola, H., Kulmala, M., Laaksonen, A., Worsnop, D. R., and
834 Laakso, L.: Chemical composition, main sources and temporal variability of PM1
835 aerosols in southern African grassland, Atmos. Chem. Phys., 14, 1909–1927, doi:
836 10.5194/acp-14-1909-2014, 2014.

837 Twomey, S.: Introduction to the Mathematics of Inversion in Remotes Sensing and
838 Indirect Measurements, Elsevier Scientific, New York, 1977.

839 Venter, A. D., Vakkari, V., Beukes, J. P., van Zyl, P. G., Laakso, H., Mabaso, D.,
840 Tiitta, P., Josipovic, M., Kulmala, M., Pienaar, J. J., and Laakso, L.: An air quality
841 assessment in the industrialised western Bushveld Ignous Complex, South Africa, S.
842 Afr. J. Sci., 108, 1059, doi: 10.4102/sajs.v108i9/10.1059, 2012.

843 Veselovskii, I., Kolgotin, A., Griaznov, V., Müller, D., Wandinger, U., and
844 Whiteman, D.N.: Inversion with regularization for the retrieval of tropospheric
845 aerosol parameters from multiwavelength lidar sounding, Appl. Opt. 41, 3685–3699,
846 2002.

847 Veselovskii, I., Kolgotin, A., Griaznov, V., Müller, D., Franke, K., and Whiteman, D.
848 N.: Inversion of multiwavelength Raman lidar data for retrieval of bimodal aerosol
849 size distribution, Appl. Opt., 43, 1180-1195, 2004.

850 Wandinger, U., and Ansmann, A.: Experimental determination of the lidar overlap
851 profile with Raman lidar, Appl. Opt., 41, 511-514, doi: 10.1364/AO.41.000511, 2002.

852 Wagner, F. and Silva, A. M.: Some considerations about Ångström exponent
853 distributions, Atmos. Chem. Phys., 8, 481-489, doi:10.5194/acp-8-481-2008, 2008.

854 Wandinger, U., Müller, D., Böckmann, C., Althausen, D., Matthias, V., Bösenberg,
855 J., Weiß, V., Fiebig, M., Wendisch, M., Stohl, A., Ansmann A., Optical and
856 microphysical characterization of biomassburning and industrial-pollution aerosols
857 from multiwavelength lidar and aircraft measurements, J. Geophys. Res., 107,
858 ~~D218~~125, doi:10.1029/2000JD000202, 2002.

859 Weinzierl B., Sauer, D., Esselborn, M., Petzold, A., Veira, A., Rose, M., Mund, S.,
860 Wirth, M., Ansmann, A., Tesche, M., Gross, S., and Freudenthaler, V.: Microphysical
861 and optical properties of dust and tropical biomass burning aerosol layers in the Cape
862 Verde region – an overview of the airborne in situ and lidar measurements during
863 SAMUM-2, Tellus, 63B, 589-618, doi: 10.1111/j.1600-0889.2011.00566.x, 2011.

Wenig, M., Spichtinger, N., Stohl, A., Held, G., Beirle, S., Wagner, T:, Jahne, B. and Platt, U.: Intercontinental transport of mitrogen oxide pollution plumes, Atmos. Chem. Phys., 3, 387-393, 2003.

Winkler, H., P. Formenti, D. J. Esterhuyse, R. J. Swap, G. Helas, H. J. Annegarn, and Andreae, M.O. : Evidence for large-scale transport of biomass burning aerosols from sunphotometry at a remote South African site: Atmos. Environ., 42, 5569-5578, doi: 10.1016/j.atmosenv.2008.03.031, 2008.

TABLES

Table 1. Aerosol type, time and altitude range of aerosol layers used for optical and microphysical aerosol characterization

aerosol source	date	time [UTC]	height [m]	Extinction Coefficient [Mm-1]	
				355 nm	532 nm
urban / industrial	25 March 2010	18:00 – 19:50	2100 – 2670	196 ± 18	75 ± 12
	25 March 2010	18:00 – 19:50	2790 – 3450	190 ± 36	68 ± 14
	25 March 2010	18:00 – 19:50	1560 – 1980 ~~– 2250~~	260 ± 6	78 ±12
	16 April 2010	21:20 – 23:54	~~2280 – 2520~~1980 – 2250	147 ± 13	58 ± 9
	16 April 2010	21:20 – 23:54	2280 – 2520	129 ± 10	39 ± 4
	16 April 2010	21:20 – 23:54	2610 – ~~3170~~3180	196 ± 43	81 ± 14
	14 May 2010	18:00 – 00:00	930 – 1360	238 ± 37	127 ± 25
	15 May 2010	18:30 – 20:20	1380 – 1860	196 ± 26	86 ± 19
	15 May 2010	18:30 – 20:20	2250 – 2700	81 ± 7	28 ± 3
	30 November 2010	17:15 – 18:00	960 – 1300	121 ± 6	44 ±13
	30 November 2010	17:15 – 18:00	1350 – 1920	146 ± 26	50 ± 11
	30 June 2010	17:00 – 18:00	1420 – 1620	101 ± 5	34 ± 5
	30 June 2010	17:00 – 18:00	1650 – 1830	71 ± 11	37 ± 7
	10 January 2011	19:15 – 20:15	1890 – 2160	303 ± 45	146 ± 31
	13 January 2011	21:00 – 22:00	1200 – 1800	342 ± 24	163 ± 17
	13 January 2011	21:00 – 22:00	1920 – 2250	267 ± 42	158 ± 29
	13 January 2011	21:00 – 22:00	2430 – 2880	199 ± 23	68 ±12
biomass burning	1 October 2010	00:10 – 01:00	1090 – 1900	331 ± 9	158 ± 8
	5 October 2010	18:10 – 23:10	1115 – 1750	432 ± 62	227 ± 37
	5 October 2010	18:10 – 23:10	1980 – 2700	256 ± 18	132 ± 15
	6 October 2010	20:00 – 00:00	1175 – 1540	277 ± 27	142 ± 5
	6 October 2010	20:00 – 00:00	1565 – 2160	214 ± 14	111 ± 11
	6 October 2010	20:00 – 00:00	2190 – 2520	152 ± 6	85 ± 16
	6 October 2010	20:00 – 00:00	2610 – 2820	121 ± 19	80 ± 6
	21 October 2010	01:30 – 02:30	880 – 1530	261 ± 28	131 ± 20
	21 October 2010	01:30 – 02:30	1685 – 2280	168 ± 7	66 ± 16
	21 October 2010	01:30 – 02:30	2400 – 2880	171 ± 30	70 ± 14
	22 August 2010	00:00 – 01.00	1205 – 1565	340 ± 13	162 ± 8
	22 August 2010	00:00 – 01.00	1685 – 1920	354 ± 5	190 ± 8
	22 August 2010	02:00 – 03:00	1115 – 1535	335 ± 6	163 ± 10
	22 August 2010	02:00 – 03:00	1745 – 2250	331 ± 15	170 ± 4
~~mixture of biomass burning & desert dust~~mixed aerosols	16 August 2010	17:00 – 18:00	1115 – 1445	316 ± 24	151 ± 9
	16 August 2010	19:00 – 20:00	995 – 1265	296 ± 7	157 ± 11
	18 August 2010	19:00 – 20:00	1175 – 1355	154 ± 9	75 ± 4
	18 August 2010	19:00 – 20:00	1415 – 1715	174 ± 11	66 ± 4
	18 August 2010	19:00 – 20:00	1865 – 2160	184 ± 6	66 ± 3
	22 August 2010	17:00 – 18:00	1145 – 1505	286 ± 3	109 ±4
	22 August 2010	17:00 – 18:00	1595 – 2040	267 ± 16	119 ± 8

Merged Cells
Inserted Cells
Formatted Table
Merged Cells
Merged Cells
Merged Cells
Inserted Cells
Inserted Cells
Formatted Table
Formatted: Font: 10 pt

Table 2. Mean value ± standard deviation of aerosol lidar ratio at 355, particle depolarization ratio and Ångström exponent related to extinction between 355 and 532 nm for the examined aerosol types, as well as value of range and median

aerosol source	mean ± stdv	range	median
lidar ratio at 355 nm [sr]			
urban / industrial	52 ± 7	41 – 59	54
biomass burning	92 ± 10	81 – 119	88
~~biomass burning & desert dust~~mixed aerosols	74 ± 11	59 – 90	~~90~~73
lidar ratio at 532 nm [sr]			
urban / industrial	41 ± 13	23 – 74	38
biomass burning	75 ± 14	47 – 92	79
~~biomass burning & desert dust~~mixed aerosols	46 ± 13	33 – 68	40
particle depolarization ratio at 355 nm [%]			
urban / industrial	0.9 ± 0.4	0.3 – 1.7	1.0
biomass burning	3.2 ± 1.3	1.2 – 5.7	2.7
~~biomass burning & desert dust~~mixed aerosols	8.3 ± 0.7	7.3 – 9.1	8.1
ångström exponent related to extinction between 355 and 532 nm			
urban / industrial	2.3 ± 0.5	1.3 – 3.0	2.4
biomass burning	1.7 ± 0.3	1.0 – 2.4	1.7
~~biomass burning & desert dust~~mixed aerosols	2.0 ± 0.4	1.6 – 2.5	2.0

Table 3. Mean value ± standard deviation of effective radius and single-sccattering albedo for the examined aerosol types, as well as range and median.

Aerosol Source	mean ± stdv	range	median
effective radius [µm]			
urban / industrial	0.10 ± 0.03	0.07 – 0.16	0.09
biomass burning	0.17 ± 0.04	0.11 – 0.28	0.17
~~biomass burning & desert dust~~mixed aerosols	0.13 ± 0.03	0.09 – 0.19	0.13
single-scattering albedo at 532 nm			
urban / industrial	0.87 ± 0.06	0.75 – 0.96	0.88
biomass burning	0.90 ± 0.06	0.77 – 0.98	0.90
~~biomass burning & desert dust~~mixed aerosols	0.88 ± 0.07	0.76 – 0.95	0.89
complex refractive index			
urban / industrial	1.61 (± 0.11) + 0.021 (± 0.010)i	1.47 – 1.78 (RRI) 0.007 – 0.039 (IRI)	1.64 (RRI) 0.020 (IRI)
biomass burning	1.43 (± 0.07) + 0.016 (± 0.011)i	1.35 – 1.57 (RRI) 0.002 – 0.046 (RRI)	1.40 (RRI) 0.015 (IRI)
~~biomass burning & desert dust~~mixed aerosols	1.52 (± 0.15) + 0.022 (± 0.015)i	1.33 – 1.74 (RRI) 0.004 – 0.046 (IRI)	1.56 (RRI) 0.019 (IRI)

Table 4. The code used in Figure 7 and the respective reference.

Code	Reference
A03	Anderson et al., 2003
A05	Ansmann et al., 2005
A09a	Ansmann et al., 2009
A09b	Amiridis et al., 2009
A11	Arboledas et al., 2011
B03	Balis et al., 2003
B12a	Baars et al., 2012
B12b	Burton et al., 2012
B13	Burton et al., 2013
G10	Giannakaki et al., 2010
G11	Groß et al., 2011
G13	Groß et al., 2013
G16	This study
H15	Hesse et al., 2015
I15	Illingworth et al., 2015
K14	Kanitz et al., 2014
K12	Kompulla et al., 2012
M05	Müller et al., 2005
M07	Müller et al., 2007
M04	Murayama et al., 2004
M13	Murayama et al., 2013
N13	Nicolae et al., 2013
P12	Preißler et al., 2012
P13	Preißler et al., 2013
R98	Reid et al., 1998
T11	Tesche et al., 2011
W02	Wandinger et al., 2002
W11	Weinzierl et al., 2011
X08	Xie et al., 2008

FIGURES

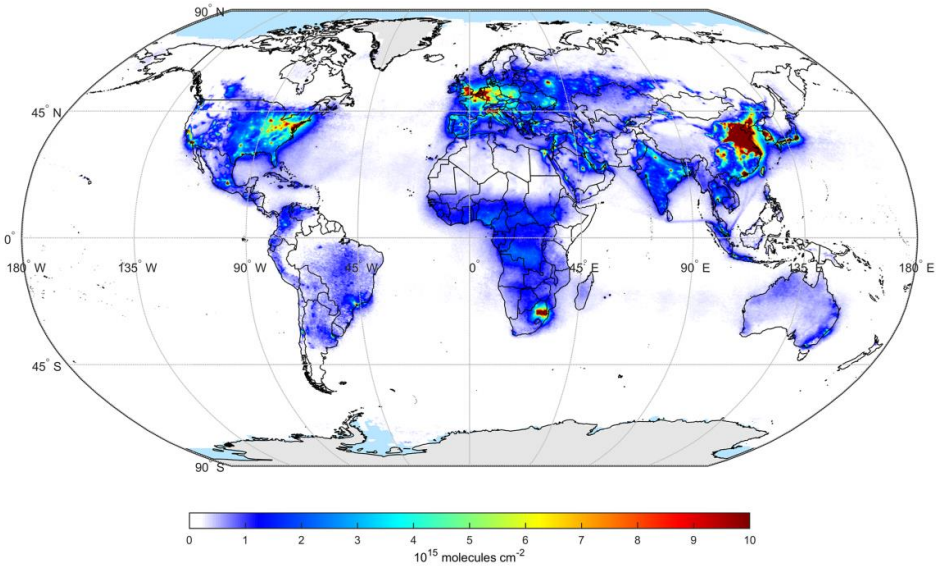

Figure 1. Global map of long-term average tropospheric NO_2 column derived from SCIAMACHY data from August 2002 to March 2012 (Schneider et al., 2015)

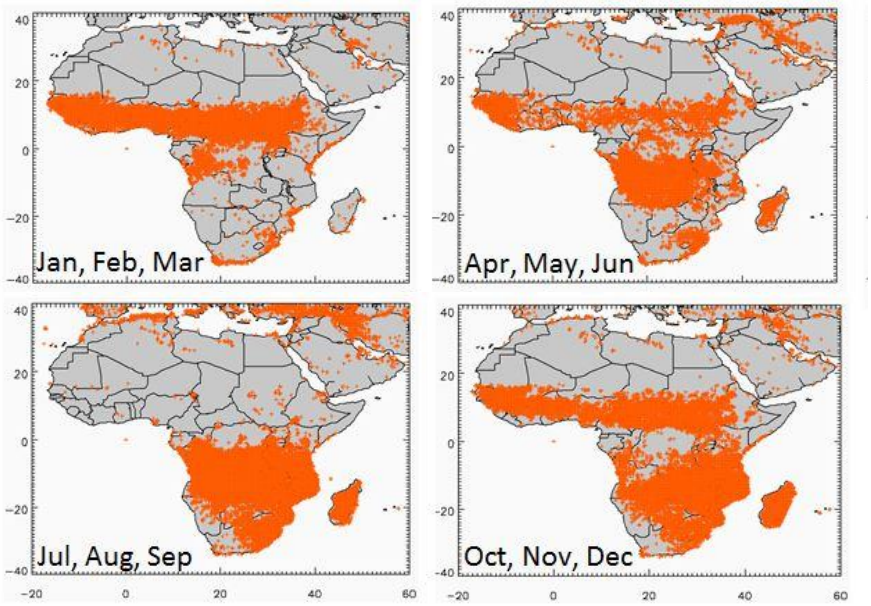

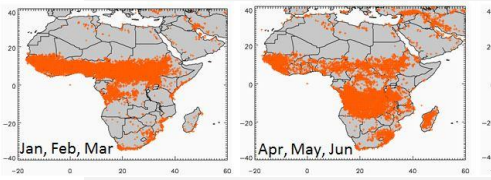

Figure 2. Number of fire hotspots with confidence levels between 80-100% averaged in terms of 3 months for the year 2010 in the latitude range between -40° and 40° and longitude range between -20° and 60°

Formatted: Font: Bold

Formatted: Justified

931
932

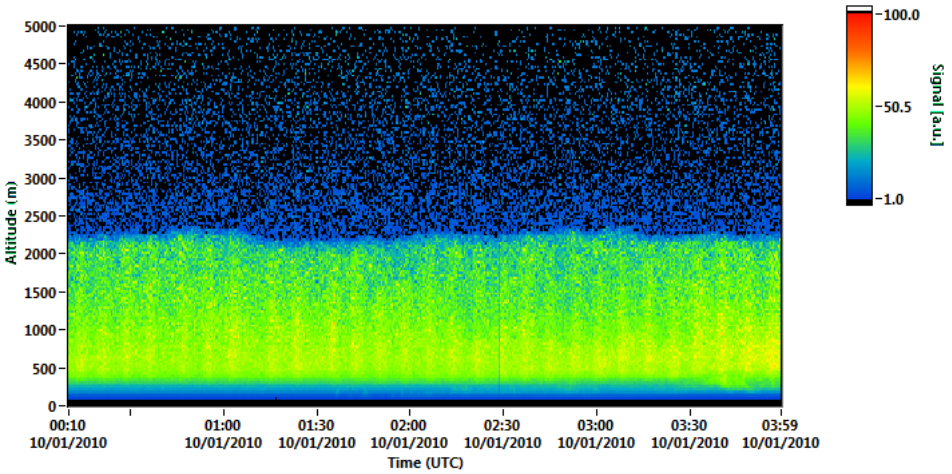
5000
4500
4000
3500
3000
2500
2000
1500
1000
500
0
Altitude (m)
00:10
10/01/2010
01:00
10/01/2010
01:30
10/01/2010
02:00
10/01/2010
02:30
10/01/2010
03:00
10/01/2010
03:30
10/01/2010
03:59
10/01/2010
Time (UTC)
100.0
50.5
1.0
Signal [a.u.]

933

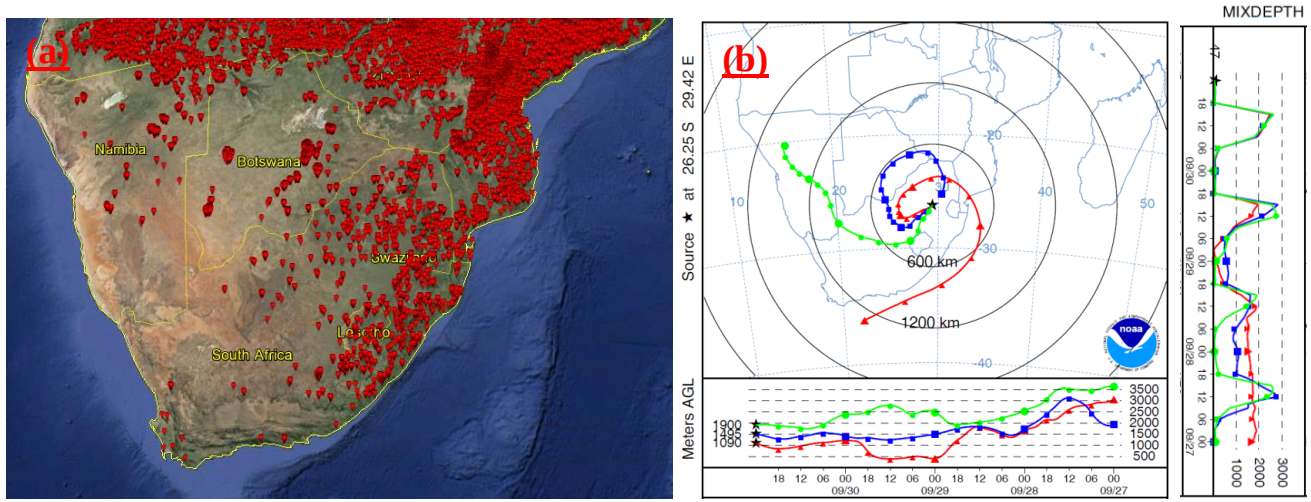

Figure 3. ~~Temporal development of the range corrected signal at 1064 nm at Elandsfontein on 1 October 2010, 00:10 – 03:59 UTC. The resolution is 15 m in height and 30 sec in time~~

Formatted: Font: Bold

Formatted: Justified

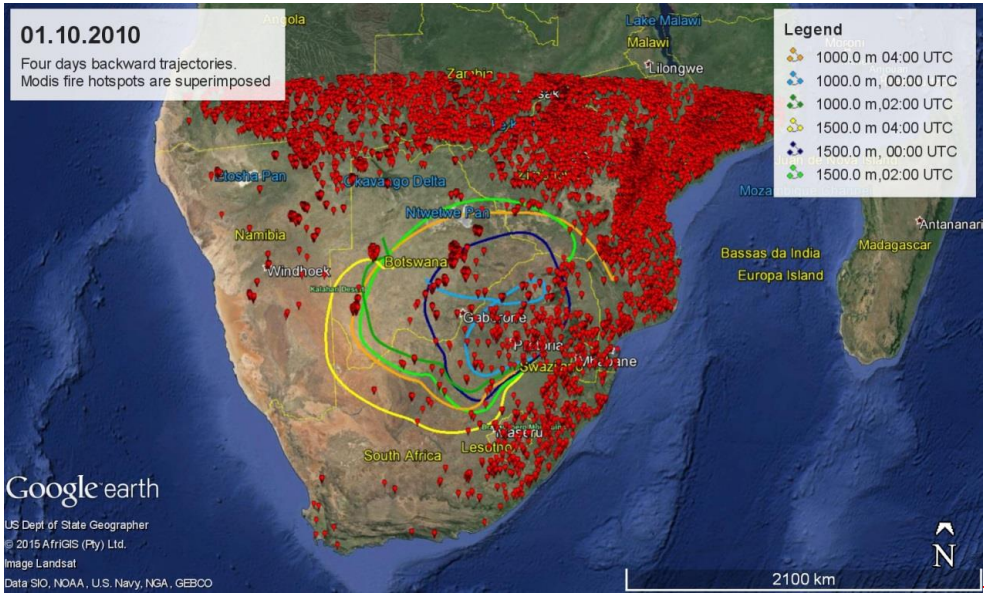

~~Figure 4.~~ ~~Four-day backward trajectories arriving at Elandsfontein on 1 October 2010 at 00:00, 02:00 and 04:00 UTC. The arrival heights above Elandsfontein are 10:00 and 15:00 UTC.~~ MODIS fire hotspots ~~are superimposed~~ for the period 28 September 2010 – 01 October 2010 and for the latitude range between -35° and -15° W and the longitude range between 10° and 40° S (a). Four-day backward trajectories arriving at Elandsfontein on 1 October 2010 at 00:00 for arrival height of the bottom (1090 m), center (1495 m) and top (1900 m) of the aerosol layer observed (b).

Formatted: Not Superscript/ Subscript

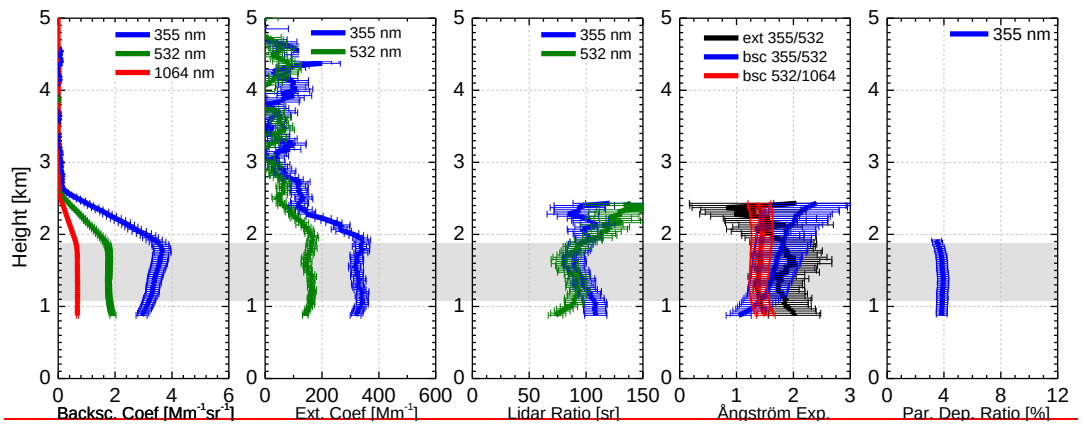
Height [km]
355 nm
532 nm
1064 nm
Backsc. Coef [Mm-1sr-1]
355 nm
532 nm
Ext. Coef [Mm-1]
355 nm
532 nm
Lidar Ratio [sr]
ext 355/532
bsc 355/532
bsc 532/1064
Ångström Exp.
355 nm
Par. Dep. Ratio [%]

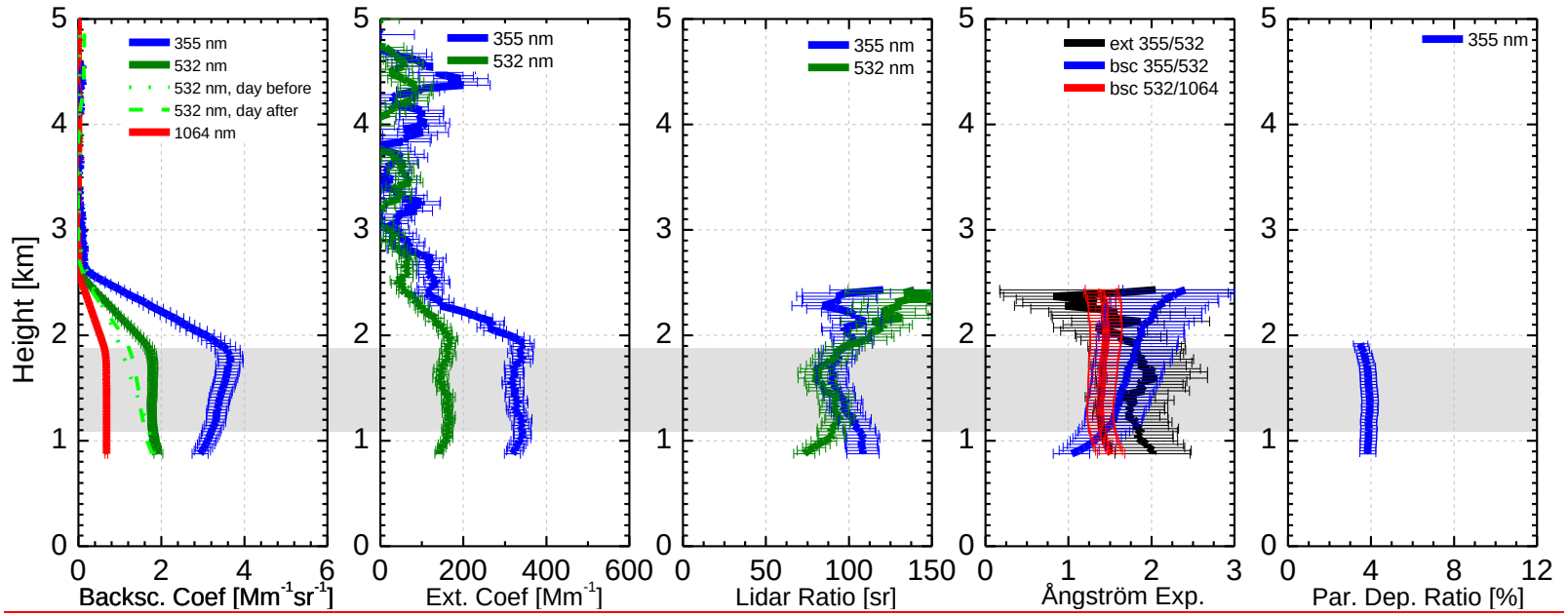

Figure ~~5~~4. Backscatter coefficients, extinction coefficients, lidar ratios, Ångstrom exponents and particle depolarization ratio at Elandsfontein on 1 October 2010, 00:10 – 03:59 UTC

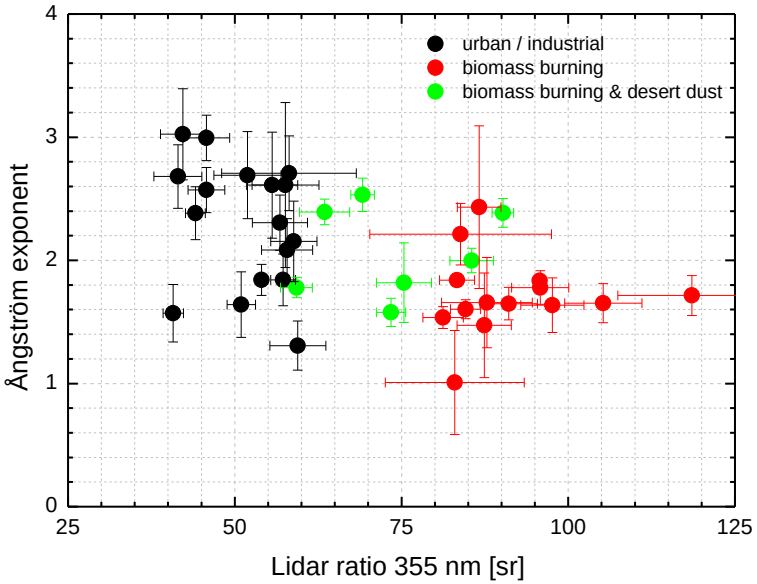
urban / industrial
biomass burning
biomass burning & desert dust
Ångström exponent
Lidar ratio 355 nm [sr]
0
1
2
3
4
25
50
75
100
125

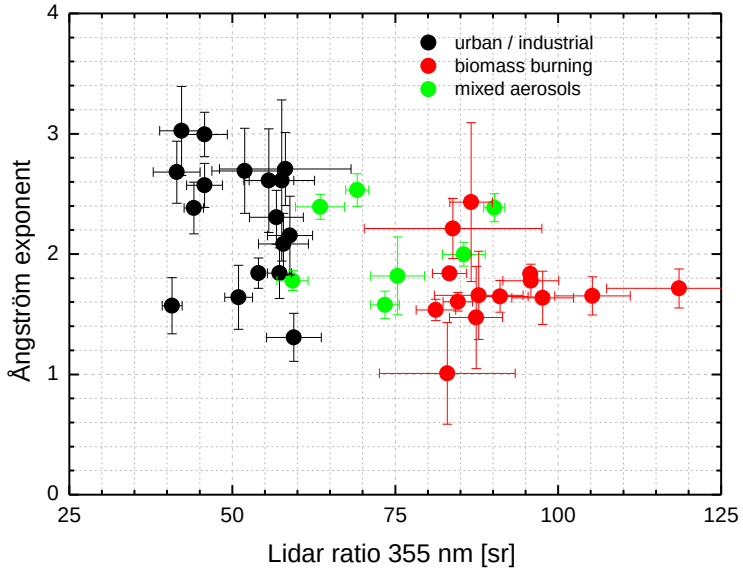

Figure ~~6~~5. Lidar ratio at 355 nm versus the extinction-related Ångström exponent from 355 to 532 nm for the three aerosol types investigated in our study

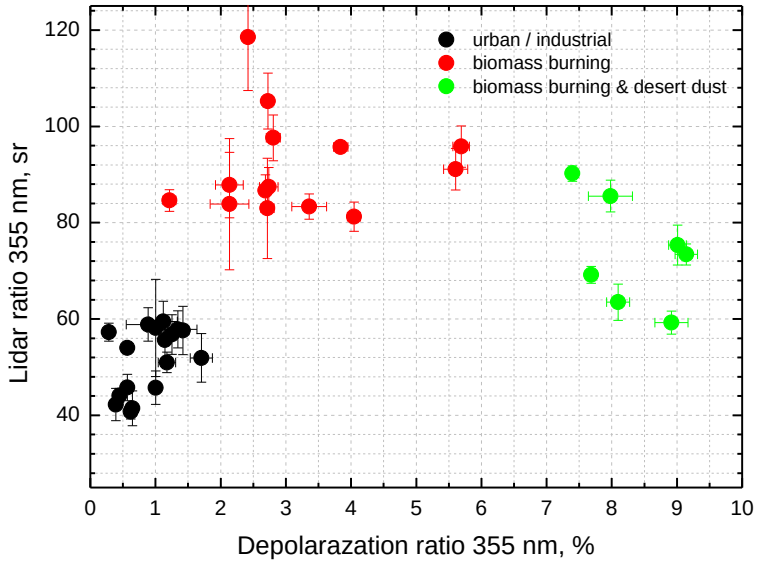

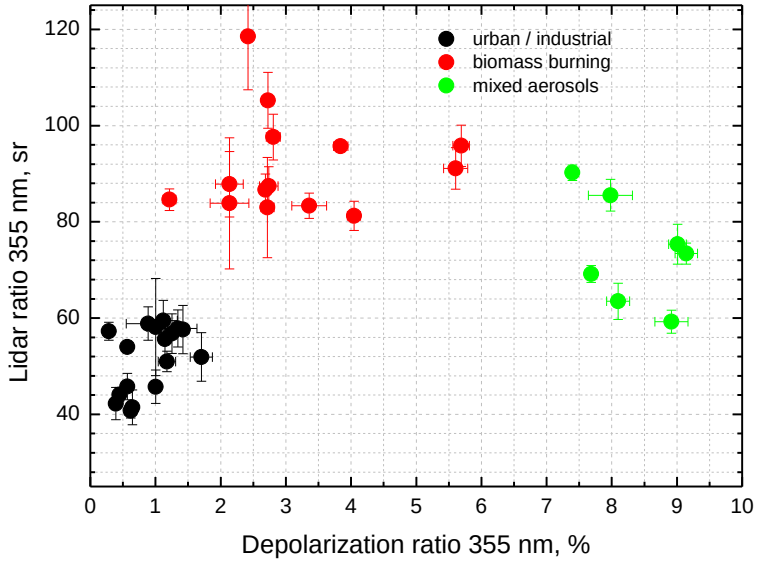

Figure ~~7~~6. Lidar ratio at 355 nm versus the depolarization ratio at 355 nm for the three aerosol types investigated in our study

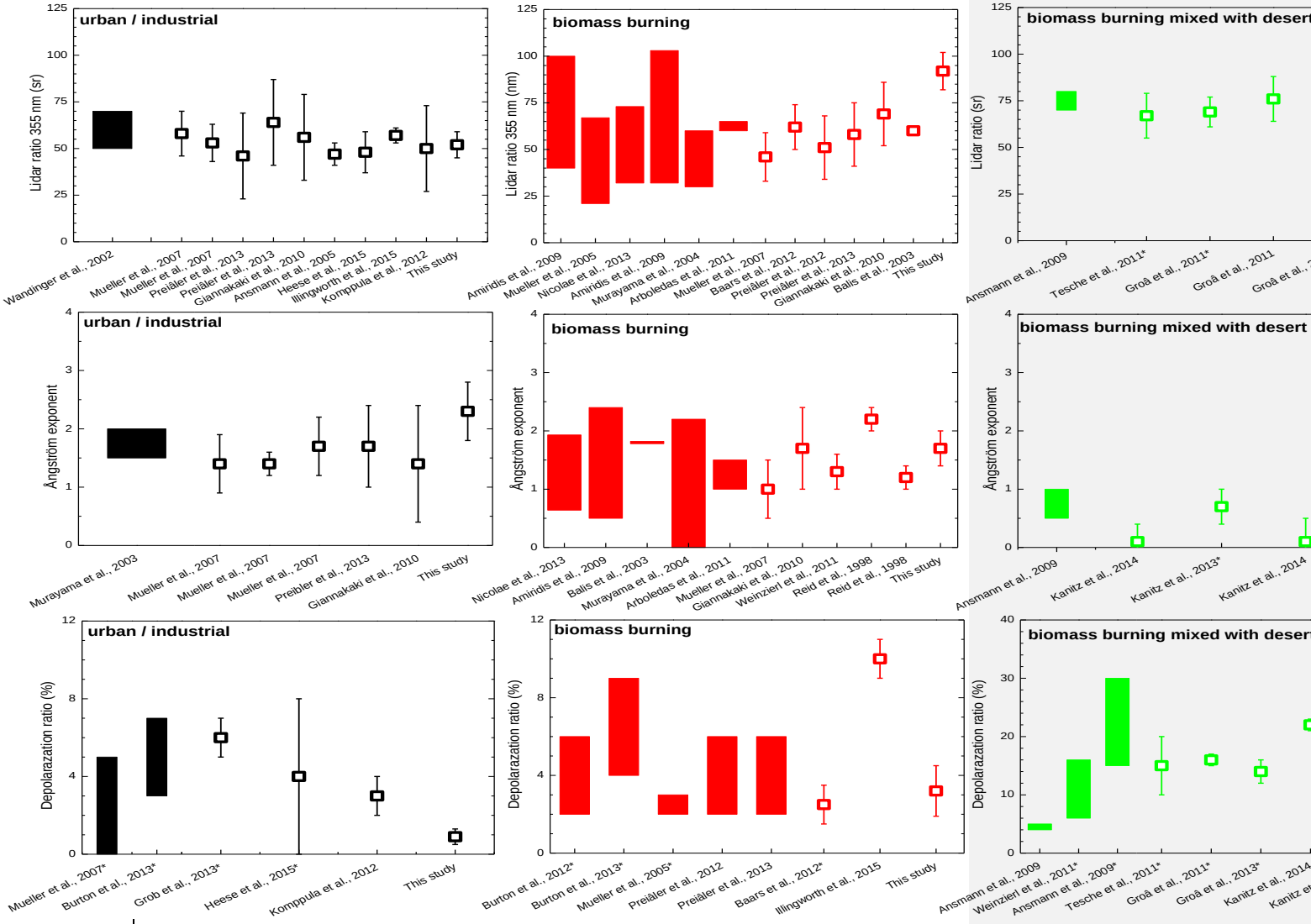
urban / industrial
biomass burning
biomass burning mixed with desert
Lidar ratio 355 nm (sr)
Lidar ratio 355 nm (nm)
Lidar ratio (sr)
Ångström exponent
Depolarazation ratio (%)
Wandinger et al., 2002
Mueller et al., 2007
Mueller et al., 2007
Preißler et al., 2013
Preißler et al., 2013
Giannakaki et al., 2010
Ansmann et al., 2005
Heese et al., 2015
Illingworth et al., 2015
Komppula et al., 2012
This study
Amiridis et al., 2009
Mueller et al., 2005
Nicolae et al., 2013
Amiridis et al., 2009
Murayama et al., 2004
Arboledas et al., 2011
Mueller et al., 2007
Baars et al., 2012
Preißler et al., 2012
Preißler et al., 2013
Giannakaki et al., 2010
Balis et al., 2003
This study
Ansmann et al., 2009
Tesche et al., 2011*
Groß et al., 2011*
Groß et al., 2011
Murayama et al., 2003
Mueller et al., 2007
Mueller et al., 2007
Mueller et al., 2007
Preißler et al., 2013
Giannakaki et al., 2010
This study
Nicolae et al., 2013
Amiridis et al., 2009
Balis et al., 2003
Murayama et al., 2004
Arboledas et al., 2011
Mueller et al., 2007
Giannakaki et al., 2010
Weinzierl et al., 2011
Reid et al., 1998
Reid et al., 1998
This study
Ansmann et al., 2009
Kanitz et al., 2014
Kanitz et al., 2013*
Kanitz et al., 2014
Mueller et al., 2007*
Burton et al., 2013*
Grob et al., 2013*
Heese et al., 2015*
Komppula et al., 2012
This study
Burton et al., 2012*
Burton et al., 2013*
Mueller et al., 2005*
Preißler et al., 2012
Preißler et al., 2013
Baars et al., 2012*
Illingworth et al., 2015
This study
Ansmann et al., 2009
Weinzierl et al., 2011*
Ansmann et al., 2009*
Tesche et al., 2011*
Groß et al., 2011*
Groß et al., 2011*
Groß et al., 2013*
Kanitz et al., 2014
Kanitz et

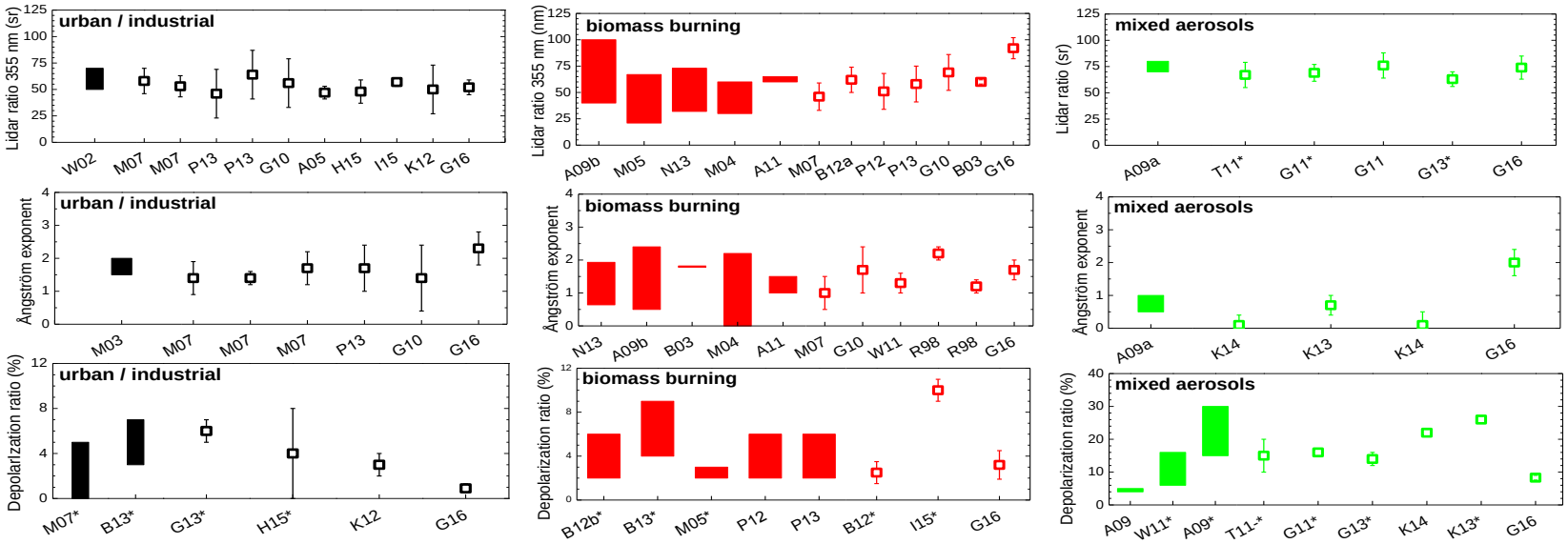

Figure ~~8~~7. General literature values for lidar ratio at 355 nm, Ångström exponent and depolarization ratio (355 or 532 nm) for urban/industrial (black), biomass burning (red) and for mixed biomass burning with desert dust aerosols (green). The x-axis are the studies presented in Table 4. Floating columns are referring to range values while the symbols are referring to mean values with one standard deviation. The depolarization values is at 355 nm except for the cases noted with asterisk (*) which are referring to visible wavelength (532 nm or 710 nm).

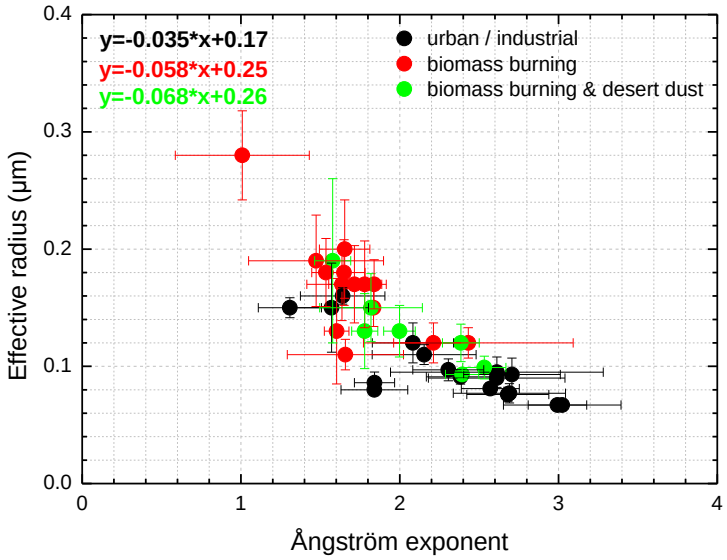
y=-0.035*x+0.17
y=-0.058*x+0.25
y=-0.068*x+0.26
urban / industrial
biomass burning
biomass burning & desert dust
Effective radius (µm)
Ångström exponent
0.0
0.1
0.2
0.3
0.4
0
1
2
3
4

Formatted

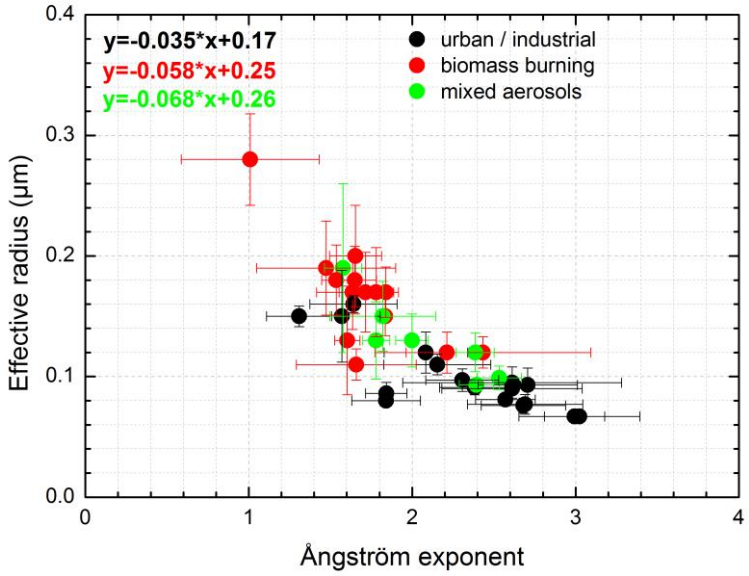

Figure ~~9~~7. Effective radius versus Ångström exponent for the three aerosol types investigated in our study.